Research Summary

John A. Gemmer

gemmerj@wfu.edu

http://users.wfu.edu/gemmerj/

Broadly, my research interests lie in applied analysis as well as in studying and developing mathematical models of phenomenon in the physical and biological sciences. As an applied mathematician, I find significant professional satisfaction studying "toy" models of systems which can yield concrete insights into phenomena observed in nature. In my work, I have developed expertise in calculus of variations, mathematical modeling, applied analysis, continuum mechanics, asymptotic methods, ordinary and partial differential equations, stochastic differential equations, dynamical systems and Riemannian geometry. A unifying theme of my work is the application of variational methods to problems in applied mathematics and interdisciplinary projects. I am also dedicated to fostering undergraduate research, and some of my published work has been done in collaboration with students. In this document, I provide a brief high level overview of my work, a more technical but still brief summary of my main results, and conclude with my plans for future research.

1 Overview of Scholarship

1.1 Main Scientific Publications

Swelling thin elastic sheets: In a sequence of works conducted primarily in collaboration with Shankar Venkataramani (University of Arizona) and experimental physicist Eran Sharon (Hebrew University of Israel), I analyzed the formation of patterns in growing thin elastic sheets. Specifically, our work in [1–5] studied the relationship between the existence and regularity of isometric immersions of two dimensional hyperbolic Riemannian manifolds in $\mathbb{R}^3$, variational models of growth, and the undulating patterns observed in leaves, swelling hydrogels, potato chips, etc. The key result of our work is the discovery of a novel type of topological defect consisting of local isometries with "lines of inflection" meeting at "branch points." While smooth isometric immersions exist, these defects were used to construct fractal like $C^{1,1}$ surfaces with lower elastic energy than their smooth counterparts. These results are surprising in that it was commonly believed that such geometric complexity results from boundary conditions or external forces that cause the sheet to buckle into approximately low regularity isometric immersions, e.g., crumpled paper, elastic ridges, d-cones. Indeed, a common argument for the formation of microstructure in such systems is that since the Euler-Lagrange equations corresponding to the elastic energy consist of a system of singularly perturbed equations, it follows that solutions will contain boundary layers in which the elastic energy is concentrated. In contrast, for hyperbolic sheets, our construction shows that while branch points and lines of inflection introduce regions of lower regularity, the elastic energy does not concentrate around these defects. The existence of such nontrivial defects plays a substantial role in the mechanics of thin hyperbolic sheets by allowing for the circumvention of the rigidity of smooth isometric immersions which further allows for a combinatorially large number of low energy states. Taken together, our results show that hyperbolic thin sheets are a very "floppy" system with fascinating geometries and mechanical properties.

Phase shaping of beams: In collaboration with experimental physicist Charles Durfee (Colorado School of Mines), Jerome Moloney (University of Arizona) and Shankar Venkataramani, I studied the problem of phase shaping beams of light into desired intensity profiles over long distances, e.g., one

kilometer. In many applications, the geometry of the initial intensity profile of a beam is fixed by the design of the laser but the spatial phase of the beam can be modified through optical instruments. The phase shaping problem is then to design the optical instruments so that the beam of light achieves a desired intensity profile along the optical axis, e.g., a Gaussian profile. The challenge with this problem is that due to its wave nature localized packets of light will broaden spatially through diffraction. Using explicit integral transform solutions of the paraxial wave equation, i.e., the linear Schrodinger equation, we posed this problem in [6] within a variational framework and used the method of stationary phase coupled with the Gerchberg–Saxton algorithm to develop a computationally efficient algorithm for obtaining the optimal phase. We expanded upon this work in [7] and proved a version of the uncertainty principle to obtain rigorous scaling laws for the optimal phase in terms of the relevant design parameters in the problem.

Image stabilization on the retina: In collaboration primarily with biologists David Berson (Brown University), Shai Sabbah (Hebrew University of Jerusalem) and Nathan Jeffery (University of Liverpool), I published a full article in *Nature* [8]. In this work, I used tools from projective geometry, continuum mechanics, and optimization theory to develop a mathematical model that was used to deduce how retinal ganglion cells and the accessory optic system encode the direction and spatial orientation of perceived objects moving in space. The challenge with this work is that cell response is not recorded from the retina's natural state (approximately spherical) but from retinas flattened on a slide. To my knowledge, our work was the first to correctly account for geometric distortions resulting from the elastic flattening. Our mathematical model was used to construct a complete mapping of direction selective cells which was compared with the optic flow resulting from the animals movement in space. Our work showed a strong correlation between the geometry of the retinal ganglion cells in mice and forward-backward motion of the animal as well as motion along the gravitational axis. While this result might not seem surprising, it is important to note that the eyes of mice are not forward facing as in humans but are on the side of the head and are slightly tilted upward. This result indicates that the orientation of direction selective cells are non-trivially oriented throughout the retina to align with common motions of the animal. While in this work I am the second author of many, most of the co-authors were lab technicians and undergraduate students who conducted the basic experimental work. The experimental design and management of the lab was conducted by my colleagues Shai Sabbah and David Berson while the three dimensional reconstruction of the animal was done by my colleague Nathan Jeffrey. I conducted all of the mathematical research, mathematical modeling, and numerical reconstruction of the retina from flat mount data.

Noise-induced tipping in periodically forced systems: In collaboration with graduate student Yuxin Chen (Northwestern University), Mary Silber (University of Chicago), and Alexandria Volkening (Purdue University), I studied the problem of determining the most probable noise-induced transition paths in periodically forced one dimensional stochastic differential equations [9]. We specifically studied the local and global minimizers of the Freidlin Wentzell (FW) and Onsager-Machlup (OM) rate functionals to determine the most probable transition paths. Within the class of the periodically forced systems we analyzed, we showed that for a forcing frequency intermediate between adiabatic and fast forcing, local minimizers of the OM functional depart the stable periodic orbits at times when the flow locally changes from expansive to compressive; thus providing a robust estimator for a time in phase space in which the system is susceptible to noise induced tipping.

Free boundary problems in polygonal domains: In collaboration with Sarah Raynor (Wake Forest University) and graduate student Gary Moon (UNC Chapel Hill), I developed and proved strong convergence of an algorithm for numerically computing solutions to an elliptic two-phase free boundary problem with Neumann fixed boundary conditions in [10]. Solutions to this problem correspond to

critical points of a functional and the algorithm relaxed the functional by mollification and exploited the variational structure to obtain solutions as a stationary point for a gradient flow. The algorithm was used to numerically explore the interaction of the free boundary with acute and obtuse corner points.

Noise-induced tipping in piecewise smooth systems: In collaboration with my postdoc Kaitlin Hill (Wake Forest) and former graduate student Jessica Zanetell (Wake Forest), I studied the problem of determining the most probable transition path in stochastic differential equations with a piecewise smooth drift. Specifically, in [11] we considered n-dimensional systems with a switching manifold that forms an $n-1$-dimensional hyperplane. Our approach was to mollify the system and consider the Γ-limit of the FW functional in the piecewise smooth limit. The resulting functional consists of the standard FW functional with an additional contribution due to times when the most probable path slides on the switching manifold. Interestingly, the additional contribution exactly vanishes for paths that follow the Filippov dynamics, i.e., the convex combination of the vector fields on either side of the switching manifold for which the normal component vanishes. This result proves, to first order in the mollification parameter, Filippov's original convex combination approach to resolve the dynamics in regions of discontinuity is the correct approach when considering the effect of additive noise.

1.2   Publications with Undergraduate Students

Brachistochrone problem in an inverse square gravitational field: In [12], under my mentorship, my former undergraduate student Chris Grimm studied the problem of determining brachistochrone curves for particles falling in an inverse square gravitational field. This problem is a nontrivial application of calculus of variations in that if only strong solutions to the corresponding Euler-Lagrange equations are considered, then it can be shown there exists a "forbidden region" through which the strong solutions do not penetrate. The novelty of this work is that by considering appropriate weak solutions constructed from local strong solutions patched together at the singular point of the gravitational field, we showed that the full space of optimal paths is more robust. In particular, these solutions enter the forbidden region and are characteristics for the Hamilton-Jacobi equation. Moreover, by also considering the inverse-square problem on an annular domain that excises the singularity at the origin, we proved that our weak solutions are recovered in the limit as the inner radius of the annulus vanishes.

Disease dynamics on adaptive networks: In [13], under my mentorship, my former undergraduate student Hannah Scanlon developed and analyzed a mathematical model for the spread of an SIR infectious disease on a network in which individuals can pause connections with infected neighbors. The novelty of this work is that we derived a mean field approximation for the density of the various node and edge states in the network. In particular, many works on modeling disease dynamics simply start from a standard system of differential equations, i.e., SIS or SIR, and introduce additional compartments, e.g., exposed (E), quarantined (Q), hospitalized (H), to account for additional complexity. However, it is often not clear how such approaches arise from the network dynamics and, moreover, they do not account for the change in the network topology as the disease progresses. Our approach differed in that our system of differential equations resulted by computing the continuum limit of a basic stochastic SIR model with an additional transition probability incorporating the pausing of edges. The resulting system can exhibit more complex phenomenon than the standard SIR model without the necessity of introducing additional compartments. Moreover, we proved that while the standard value for the basic reproductive number R_0 is identical to the classic SIR model, there are additional parameter regimes in which the severity of the epidemic is drastically reduced. This result provides criteria beyond $R_0 < 1$, namely different criteria on the pausing rate for controlling the spread of an infectious disease.

2   Scientific Contributions

2.1   Swelling Thin Elastic Sheets

The rippling patterns observed in swelling hydrogels, leaves, and torn plastic provide striking examples of periodic and self-similar patterns; see Fig.1. One model of growing thin elastic sheets is the non-Euclidean model of elasticity which posits that growth permanently deforms the intrinsic distance between material points. Material points on the center surface are labelled by $(x, y) \in \Omega$, a subset of $\mathbb{R}^2$, and the natural distances between points in the center surface are encoded in the arc length element:

$$ds^2 = g_{11}(x, y)dx^2 + 2g_{12}(x, y)dxdy + g_{22}(x, y)dy^2, \tag{1}$$

with g_{ij} the components of a Riemannian metric $\mathbf{g}$ [14–16]. That is, the Riemannian metric $\mathbf{g}$ models the growth process by encoding the distorted strain free distance between material coordinates. By the Kirchoff hypothesis [17], the conformation of the sheet as a 3-dimensional object in $\mathbb{R}^3$ is determined by an immersion $F : \Omega \to \mathbb{R}^3$ of the center surface. By Gauss's Theorema Egregium, $\mathbf{g}$ generates an intrinsic definition of Gaussian curvature K throughout the sheet. Locally, $K < 0$ ($K > 0$) corresponds to the regions in which local growth (atrophy) occurs in the sheet. In this framework, the elastic energy is then modeled as the sum of stretching and bending contributions:

$$E[F] = \mathcal{S}[\nabla F] + t^2 \mathcal{B}[D^2 F] = \int_\Omega \|(\nabla F)^T \cdot \nabla F - \mathbf{g}\|^2 \, dxdy + t^2 \int_\Omega \left(k_1^2 + k_2^2\right) \, dxdy, \tag{2}$$

where t is the thickness of the sheet and k_1, k_2 are the principal curvatures of F [14, 18].

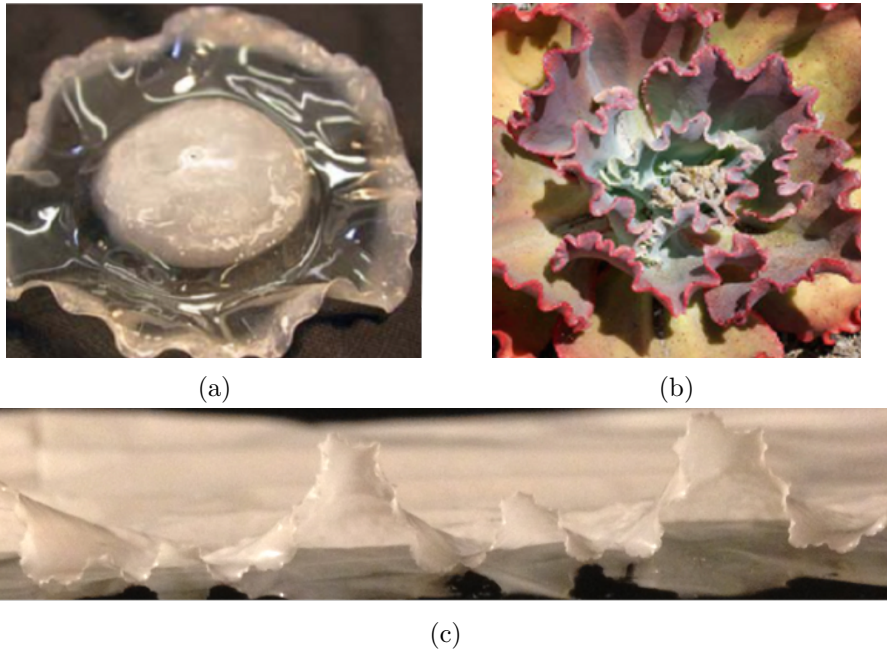(a)   (b)

(c)

Figure 1: Examples of periodic and self-similar wrinkling patterns in swelling thin elastic sheets. (a) Hydrogel disk with non-uniform swelling pattern. (b) Ornamental echeveria plant. (c) Edge of a torn trash bag.

Due to the relative strength of stretching to bending rigidity, it is natural to expect that thin sheets deform into low bending energy configurations that remove all in-plane strain. This corresponds to the "restricted" problem of minimizing the bending energy over all *isometric immersions* of the Riemannian 2-manifold $(\Omega, \mathbf{g})$, i.e., deformations satisfying $(\nabla F)^T \cdot \nabla F = \mathbf{g}$. Indeed, provided they

exist, finite bending energy isometric immersions of $(\Omega, \mathbf{g})$ are the $t \to 0$ limits of minimizers of the "full" elastic energy (2) [19]. For K uniformly negative, however, the extrinsic geometry of the system imposes that with increasing domain size smooth isometries will develop singularities where one of the principal curvatures diverges [20] and for $K = -1$ these singularities form curves – "singular edges" – across which the bending energy diverges [21]. Moreover, the Nash embedding theorem guarantees the existence of at least C^1 regular isometric immersions [22], but these surfaces are too rough to be candidates for a minimizer. A natural question then is: What is the behavior of minimizers of the elastic energy given the constraints on the regularity of isometric immersions for hyperbolic metrics?

2.1.1   Sheets with constant negative Gaussian curvature

In [1] we studied this problem for growth profiles with corresponding constant negative Gaussian curvature K_0. In this setting, the problem of studying the elastic energy of isometric immersions reduces to analyzing the behavior of solutions to the sine-Gordon equation:

$$\frac{\partial^2 \phi}{\partial x \partial y} = -K_0 \sin(\phi), \tag{3}$$

where ϕ, restricted to lie in the set $[0, \pi]$, is the angle between coordinate curves in a Chebychev net (C-net) parametrization [23]. By considering smooth solutions to Eq.(3), we showed that the principal curvatures of smooth isometric immersions satisfy the following scaling law:

$$\max\{|k_1|, |k_2|\} \geq \frac{1}{64} \exp\left(|K_0|^{\frac{1}{2}} R\right), \tag{4}$$

where R is the diameter of the domain Ω. This scaling law emphasizes that, with increasing domain size, it becomes prohibitively expensive to maintain smoothness and the isometry constraint. By explicit construction, we showed that an energetically favorable alternative is for the sheet to introduce mild singularities in the form of lines of inflection to obtain n-periodic "monkey saddles." Specifically, these isometries are formed by solving Eq.(3) with boundary conditions that enforce the C-net parameterization to contain two straight asymptotic lines that intersect at the origin. By taking odd periodic reflections about these lines, the monkey saddles can be constructed; see Fig.2(a). These monkey saddles are not smooth – every smooth isometry locally has the shape of a saddle – but nevertheless are finite bending energy isometric immersions, i.e., $W^{2,2}$ isometric immersions. In particular, as illustrated in Fig.2(b), for moderate domain sizes these isometries have lower elastic energy than their smooth counterparts. Moreover, these shapes qualitatively agree with controlled experiments on hydrogels with constant Gaussian curvature [24]; see Fig.2(c).

Fig.2(c) indicates that, for constant Gaussian curvature, the sheets adopt increasingly complex shapes with decreasing thickness. In $[1, 2]$, we analyzed this phenomenon within the "small-slope" regime. Namely, defining the small parameter $\epsilon = \sqrt{|K_0|}R$, we assumed an in-plane and out-of-plane *ansatz* of the form

$$F = i + \sqrt{K_0} i_\perp \circ \eta + K_0 i \circ \chi, \tag{5}$$

where $\chi \in W^{1,2}(\Omega, \mathbb{R}^2)$, $\eta \in W^{2,2}(\Omega, \mathbb{R})$, $i : \mathbb{R}^2 \mapsto \mathbb{R}^3$ is the standard immersion and $i_\perp$ maps into the orthogonal compliment of $i(\mathbb{R}^2)$. Keeping terms only up to order ϵ^2, the solvability condition for the existence of an isometric immersion is the following Monge-Ampere equation:

$$\det(D^2 \eta) = -1. \tag{6}$$

Eq.(6) can be solved explicitly by assuming $\eta = ax^2 + bxy + cy^2$ which reduces the differential equation to the simple algebraic equation $4ac - b^2 = -1$. The global minimum of the elastic energy is obtained by the harmonic function $\eta = xy$ which corresponds to a minimal surface within the small-slope
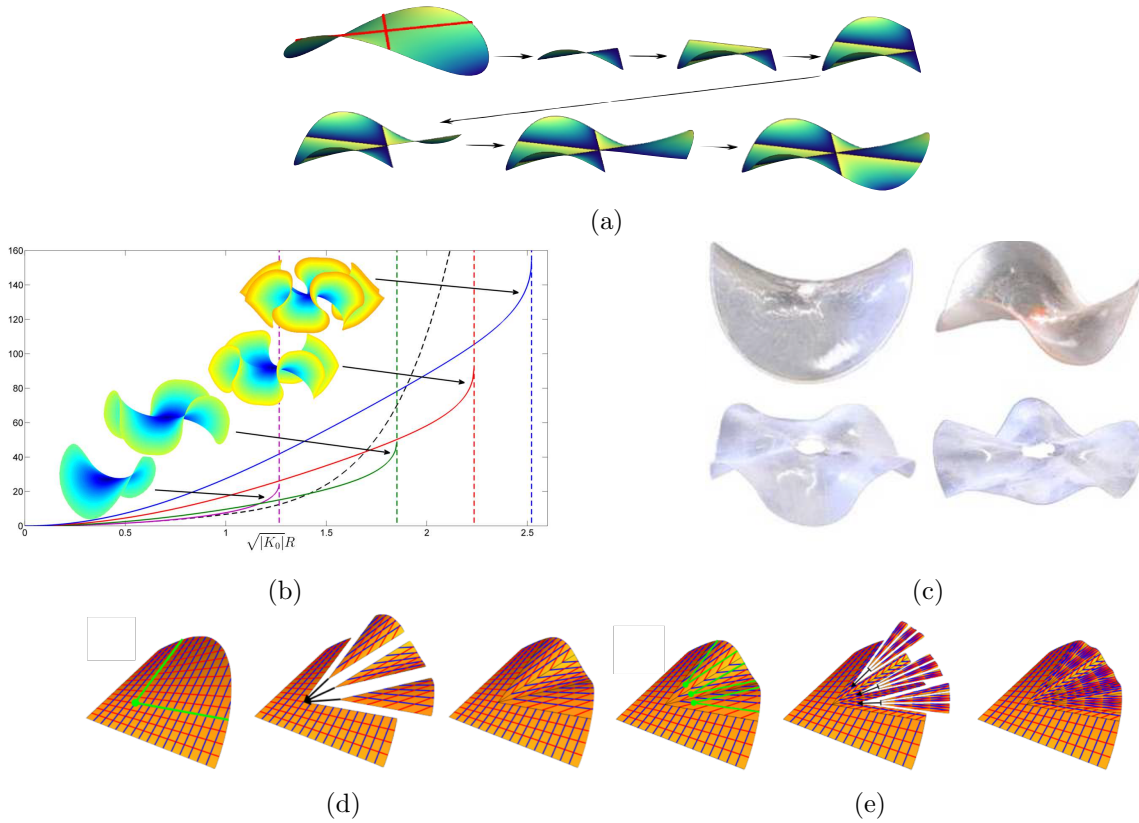
Figure 2: (a) One parameter family of isometric immersions formed by taking odd periodic extensions of solutions to Eq.3 about lines of inflection. (b) The bending energy of n-wave ($n = 2, 3, 4, 5$) piecewise smooth isometric immersions of constant Gaussian curvature K_0. The vertical dashed lines correspond to the radius where the bending energy diverges. The dashed curve corresponds to the optimal bending energy for smooth isometric immersions (c) Hydrogel disks with constant radius $R = 14mm$, constant Gaussian curvature $K_0 = -.0011mm^{-2}$ and varying decreasing thickness clockwise from the upper left [24]. (d-e) Three and nine sub-wrinkle solutions created by inserting rotated and translated copies of solutions to Eq.(6) onto the solution $\eta = xy$.

.

approximation. As above, n-wave monkey saddle solutions to Eq.(6) can also be constructed by introducing lines of inflection and taking odd periodic reflections. Moreover, in [4], we showed that these types of defects can be introduced in the sheet not at just the origin but at generic "branch points" by inserting rotated and translated copies of solutions to Eq.(6) in such a manner that the isometric immersion remains $W^{2,2}$; see Fig.2(d-e). This process can be done in a self-similar manner to at least qualitatively reproduce the patterns observed in torn plastic. However, using *a priori* estimates we proved in [2] that the full elastic energy satisfies the scaling law

$$cnt^2 \leq \inf E[F] \leq Cn^2t^2 \tag{7}$$

in the small-slope regime. This result quantifies the tradeoff in energy that occurs by increasing the number of waves in the profile and proves that in the small-slope regime for sheets with constant Gaussian curvature there can be no refinement of the wavelength of minimizers with decreasing thickness.

2.1.2   Spatially varying Gaussian curvature

In [4,5], we extended our analysis from the constant curvature case to problems with spatially varying Gaussian curvature. Namely, we studied the following Monge-Ampere equation:

$$\det(D^2\eta) = -\frac{f''(y)}{2}, \tag{8}$$

where f is a positive, monotone decreasing, concave function that models localized swelling near the edge of the domain. For $p > 0$, we found explicit solutions to this equation for $f(y) \sim (1 + y/l)^{-p}$ and $f(y) \sim \exp(-y/l)$ where $l > 0$ is a length scale associated with the swelling. Similar to the construction for constant negative curvature, we show that periodic solutions to Eq.(8) can be constructed by odd extension across lines of inflection that have lower energy than their smooth counterparts. However, in this case we showed by explicit construction that the introduction of branch points drastically lowers the elastic energy of the sheet. The numerical algorithm for constructing these piecewise smooth isometric immersions was published in [5].

One of the key insights of our work was to introduce a dimensionless geometric quantity $\eta = H/\sqrt{|K|}$, termed the disparity, which quantifies the local contribution to the bending content of the sheet arising from the mismatch in the principal curvatures. In regions in which solutions of Eq.(8) has a large disparity, it was energetically favorable to introduce a branch point to lower the elastic energy; see Fig.3(a). Indeed, by comparing the elastic energy of sheets we showed that it is energetically favorable to introduce branch points as the size of the domain increase; see Fig.3(b). This result highlights the fact that these defects are unique in that they do not concentrate elastic energy in the vanishing thickness limit. They arise to bypass the geometric rigidity of smooth isometric immersions which prevents the refinement of the pattern wavelength. To our knowledge, this is the first example of a condensed-matter system whose morphology is driven by geometric rather than energetic defects.
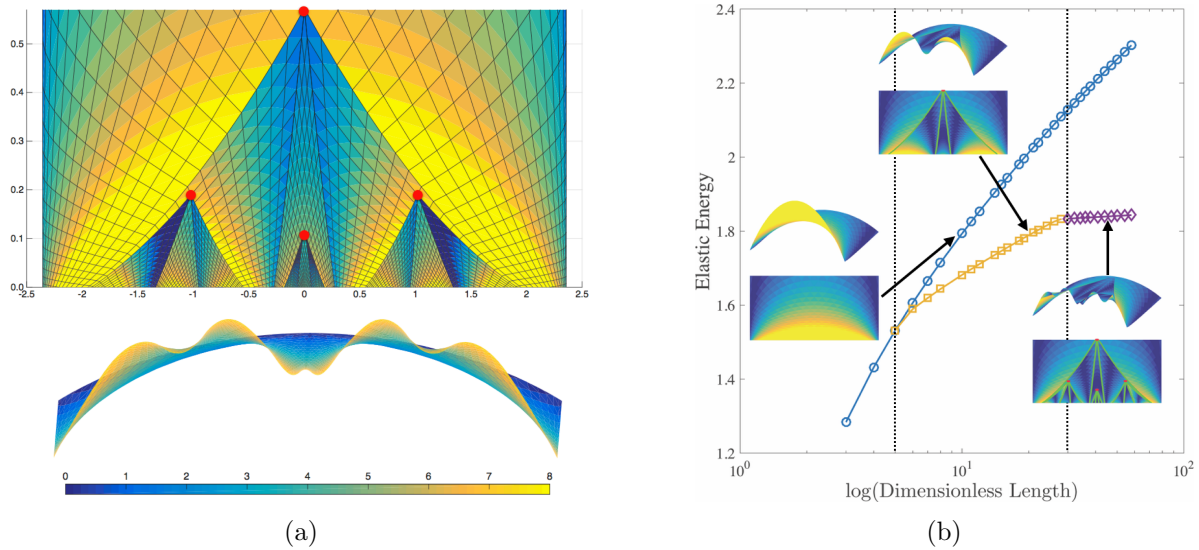

(a)   (b)

Figure 3: (a) Four-branch-point isometric immersion for the growth profile $f(y) = (1 + y/l)^{-1}$. The surface is colored by the local disparity η. (b) Comparison of the elastic energy between isometric immersions containing no branch points, one branch point, and four branch points.

2.2   Phase Shaping of Beams

In many applications, it is desirable to shape a beam or pulse of light so that it has specific properties along the optical axis. In particular, for applications in microscopic imaging [25], optical tweezers [26],

laser micro-machining [27], dressing of optical filaments [28], filament formation [29], and long-range laser ablation [30, 31], to name a few, it is important to have a well-controlled beam with a nearly uniform intensity along the optical axis. However, due to its wave nature localized packets of light will broaden spatially through diffraction. For example, Gaussian beams of width W_0 and wavenumber k double in spatial extent over the Rayleigh range $z_R \sim W_0^2 k/2$ [32]. In [6,7], we studied the problem of "beating" the Rayleigh range by applying a radially symmetric phase function $\phi(r)$ at the input plane $z = 0$ to focus a ring beam intensity profile $E_0 f(r)$ of radius r_0 and width W_0 onto a target intensity profile $E_T F_T(z)$ of width W_T along the optical axis centered at a target distance z_d; see Fig 4.
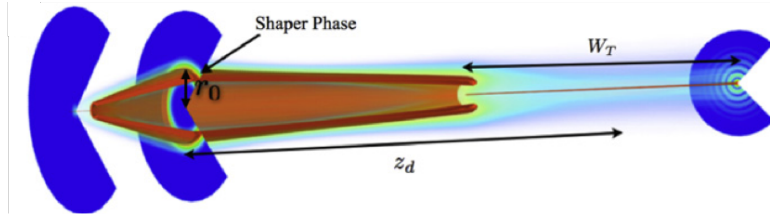

Figure 4: A schematic diagram for the geometry of the beam shaping problem.

In our work, we reformulated this optical design problem in terms of a minimization problem for the following functional:

$$I[\varphi] = \|G(\Omega) - |\mathcal{F}[g(s)\exp(i\varphi(s))](\Omega)|\,\|_{L^2}, \tag{9}$$

where g and G are given positive compactly supported functions, $\mathcal{F}$ denotes the Fourier transform, and the minimization is over the space $\mathcal{M}$ of measurable functions on $\mathbb{R}^+$. This problem is closely related to the problem of phase retrieval from two intensity measurements, i.e., the problem of determining the complex argument of a function given both knowledge of the modulus of a function and the modulus of its Fourier transform. Within the context of phase retrieval, the most common technique for optimizing I is the alternating projection algorithm pioneered by Gerchberg and Saxton [33] and its variants, such as the hybrid input-output algorithm developed by Fienup [34].

The original Gerchberg-Saxton (GS) is an error reducing algorithm in the sense that $I[\varphi_{n+1}] \leq I[\varphi_n]$. However, this property alone does not guarantee convergence of the algorithm. In particular, while projection algorithms converge when the projections are onto convex sets [35,36], for fixed s on Ω the projections employed by the GS algorithm are equivalent to projections onto the boundary of the unit ball in $\mathbb{C}$ which is clearly not convex. This lack of convexity commonly leads to stagnation of the algorithm away from the global minimum which must be overcome by additional ad hoc means [37–39]. However, while in phase retrieval it is clear that the minimum value is zero, for the optimization problem we considered this is not the case and, in fact, the minimum may be significantly bounded away from zero. Therefore, when applied to this variational problem it is not clear *a priori* what a sufficient convergence criterion for the GS algorithm would be.

In [6,7] we developed an adapted version of the GS algorithm to avoid this stagnation issue. Namely, we used the method of stationary phase to reduce the problem of creating an accurate guess for the GS algorithm to that of solving an initial value problem. The solution to this initial value problem provides a very accurate *ansatz* for the optimal phase in the short wavelength limit $k r_0 W_0 W_T / z_d^2 \gg 2\pi$. Moreover, using essentially the uncertainty principle, we proved *ansatz free* lower bounds on the minimum value of this functional which quantify that a necessary condition for accurate beam shaping is that

$$\beta = \frac{2k W_T W_0 r_0}{4z_d^2 - W_T^2} > \pi. \tag{10}$$

The central result of our work is the identification of the dimensionless quantity β's critical role in

determining the accuracy and applicability of phase shaping in term of the design parameters. Namely, we identified three scaling regimes:

1. For $\beta \ll \pi$, the uncertainty principle guarantees that neither the GS algorithm nor any other numerical algorithm will yield accurate shaping of the beam.

2. For $\beta \gg \pi$, the method of stationary phase yields a very accurate approximation to the optimal shaper phase. This asymptotic regime can be considered within the geometrical optics setting in the sense that light rays originating from the input plane are accurately mapped to the target intensity profile.

3. For $\beta \sim \pi$, the phase produced by the method of stationary phase is significantly improved upon by the GS algorithm. However, a universal scaling law for the error in terms of the wavelength is not possible.

2.3   Image Stabilization on the Retina

When animals move in space, visual feedback and stimulus from otolithic organs and the semicircular canals within the inner ear drive image stabilization and head movements [40, 41]. On the retina, movement through space induces a vector field with the corresponding optic flow detected through stimulation of ON-OFF direction sensitive ganglion cells (ON-OFF-DSGCs). Specificaly, ON-OFF-DSGCs are a type of neuron that becomes excited by optic flow from a specific direction [42, 43]. A natural question to ask is how are the ON-OFF-DSGCs distributed in the retina so that they can process the spherical geometry of the optic flow.

In [8], I worked with an interdisciplinary team to address this question by developing a mathematical model for optical flow that could be compared with *in-vitro* measurements of the position and direction sensitivity of ON-OFF-DSGCs. However, given that such measurements are conducted on flat mounted retinas, an elastic model for the flattening of the retina was needed to accurately map the recorded data back to the spherical retina. To do so, I modeled the retina as a truncated sphere $\mathcal{S}$ of radius R and maximal longitudinal distance M with four cuts made along lines of longitude. The retina was parameterized by a map $\mathbf{x}$ with domain of parameterization Ω, whose local coordinates are given by arc-length s as measured from the south pole and θ the azimuthal angle. The four relieving cuts were assumed to lie along meridians so that Ω can be decomposed into four sectors Ω_i. The flat-mounted retina from which data was collected was modeled by a domain $\mathcal{D} \subset \mathbb{R}^2$, and the flattening of the retina was modeled by a mapping $F : \Omega \mapsto \mathcal{D} \subset \mathbb{R}^2$ that minimized an appropriate elastic energy. Specifically, we assumed the retina was an isotropic, incompressible, elastic material with linear stress-strain constitutive relationship and modeled the per-unit thickness elastic energy of a flattening map $F \in W^{1,4}(\Omega, \Omega')$ by

$$E[F] = \sum_{i=1}^{4} \int_{\Omega_i} \left[\nu \left(\gamma_{11} + \gamma_{22} \right)^2 + (1 - \nu) \left(\gamma_{11}^2 + 2\gamma_{12}^2 + \gamma_{22}^2 \right) \right] \sin\left(\frac{s}{R} \right) ds d\theta, \tag{11}$$

where $\nu = 1/2$ is the Poisson ratio for the material, γ_{ij} is the intrinsic in-plane strain tensor that accounts for the curvature of the sphere, and the summation is over each sector of the retina as defined by the cuts. The optimization of this energy was performed using a Rayleigh-Ritz type algorithm. To compare data across retinas, all cells were mapped to a standard flat mounted retina $\mathcal{D}'$ which was constructed assuming an ideal retina with equally spaced cuts of equal length; see Fig.5(a) for a schematic of the various mappings as well as a numerical reconstruction of a flat mounted retina.

Translatory and rotatory optic flow on the retina was generated by first computing the corresponding flow on an arbitrary sphere $\mathcal{S}'$ in the far field and using geometric optics with the cornea acting as a lens to focus the vector field onto the retina. In the jargon used within this field of research,
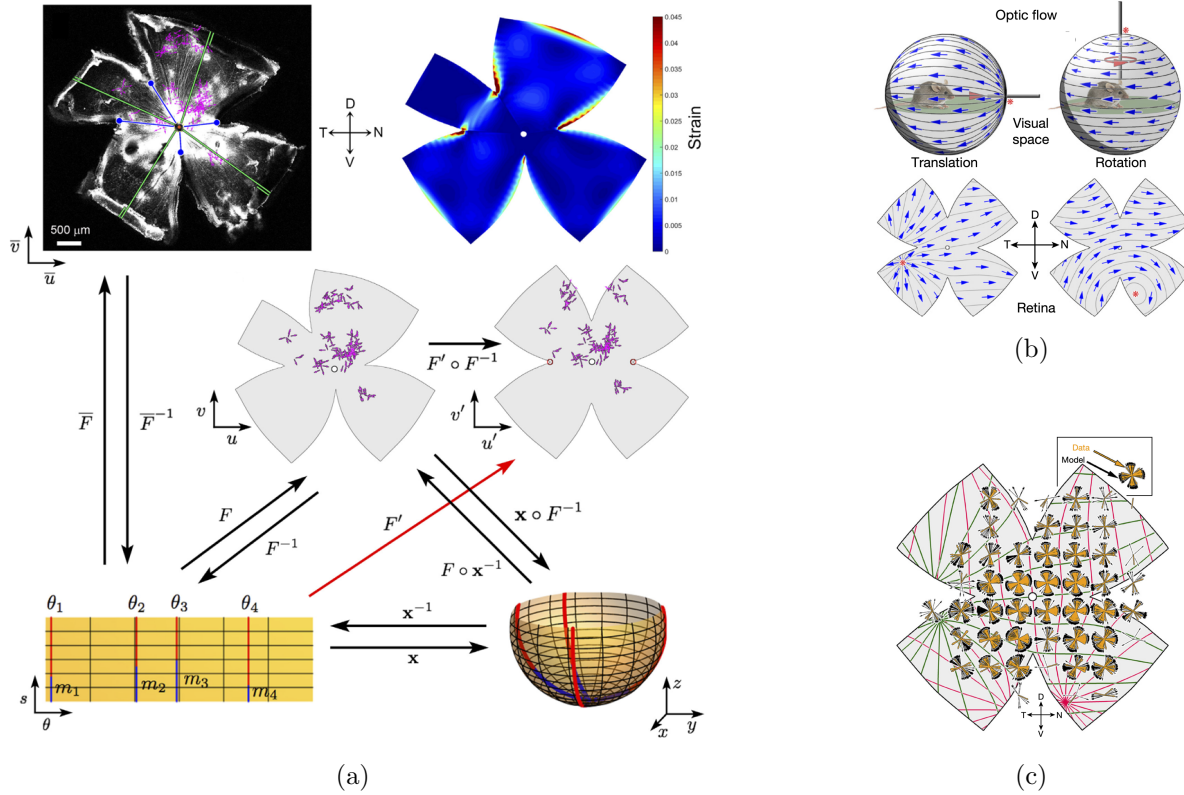
Figure 5: (a) Schematic diagram of the various mappings of a flat mounted retina. In vitro measurements of the position and orientation of ON-OFF-DSGCs (upper left inset figure) are mapped to a numerically constructed flat mounted retina and a standard flat mounted retina (middle grey inset figures). The upper right inset figure corresponds to the numerically computed reconstructed retina colored by local strain. The bottom two inset figures correspond to the domain of parameterization for the spherical retina as well as the spherical representation of the retina. (b) Translatory and rotatory optic flow in extrapersonal space generated by forward motion and cervical rotation of the head respectively with the corresponding optical flow mapped to the retina. (c) The two best fitting optical flows compared with the measured ON-OFF-DSGC response.

$\mathcal{S}'$ is called extrapersonal person but is equivalent to a subset of real projective space $\mathbb{RP}^2$, i.e., the set of lines through the origin of the eye that lie within the visual range. In spherical coordinates $(\hat{\phi}, \hat{\theta}) \in [0, \pi] \times [0, 2\pi]$ on $\mathcal{S}'$, the vector fields corresponding to translatory and rotatory optic flow about a point $(\hat{\phi}_0, \hat{\theta}_0)$ are then computed as the push forward of standard vector fields, e.g., translatory and rotatory vector fields centered on the optical axis, under the appropriate Euler angle rotation matrix; see Fig.5(b). The optical flow generated by such vector fields was then compared with the direction sensitivity gathered from the experimental data pooled onto the standard retina; see Fig.5(c). By optimizing the origin points $(\hat{\phi}_0, \hat{\theta}_0)$ with respect to an L^2 norm, I deduced the optical flow that best fits the measured data; see Fig.5(c). The existence of two optimal optical flows corresponds to the fact that there are four types of ON-OFF-DSGCs but two of the types correspond to the opposite orientation of the others. Through a full three dimensional reconstruction of the mouse, we showed that the ON-OFF-DSGCs are distributed throughout the retina to align with forward-backward motion of the animal as well as motion along the gravitational axis.

2.4   Noise-induced tipping in periodically forced systems

Motivated by applications with intrinsic seasonal forcing, e.g., sea ice extent [44, 45] or yearly disease outbreaks [46], in [9] we studied the problem of characterizing noise induced tipping events in periodically forced systems. To do so, we focused on a system in which we could directly modify the time scales in the problem:

$$dx_t = \frac{1}{\varepsilon} f(x_t, t) + \sigma dW_t = \frac{1}{\varepsilon} \left(x_t - x_t^3 + \alpha + A\cos(2\pi t) \right) dt + \sigma dW_t. \tag{12}$$

Here $x_t \in \mathbb{R}$, W_t is the standard Wiener process, $\varepsilon > 0$, and $\alpha, A, \sigma \geq 0$ are parameters chosen so that the deterministic skeleton of Eq.(12) has two stable periodic orbits separated by an unstable one. In particular, the parameter ε represents a ratio of the characteristic relaxation time to equilibrium to the period of the forcing and governs whether the system can be thought of as lying in an adiabatic, fast forcing, or intermediate regime; see Fig.6(a). While the adiabatic regime has been the focus of many studies [47–51] and in the fast forcing regime the periodicity can be removed through averaging [52,53], the intermediate forcing regime has been the subject of few studies [54].
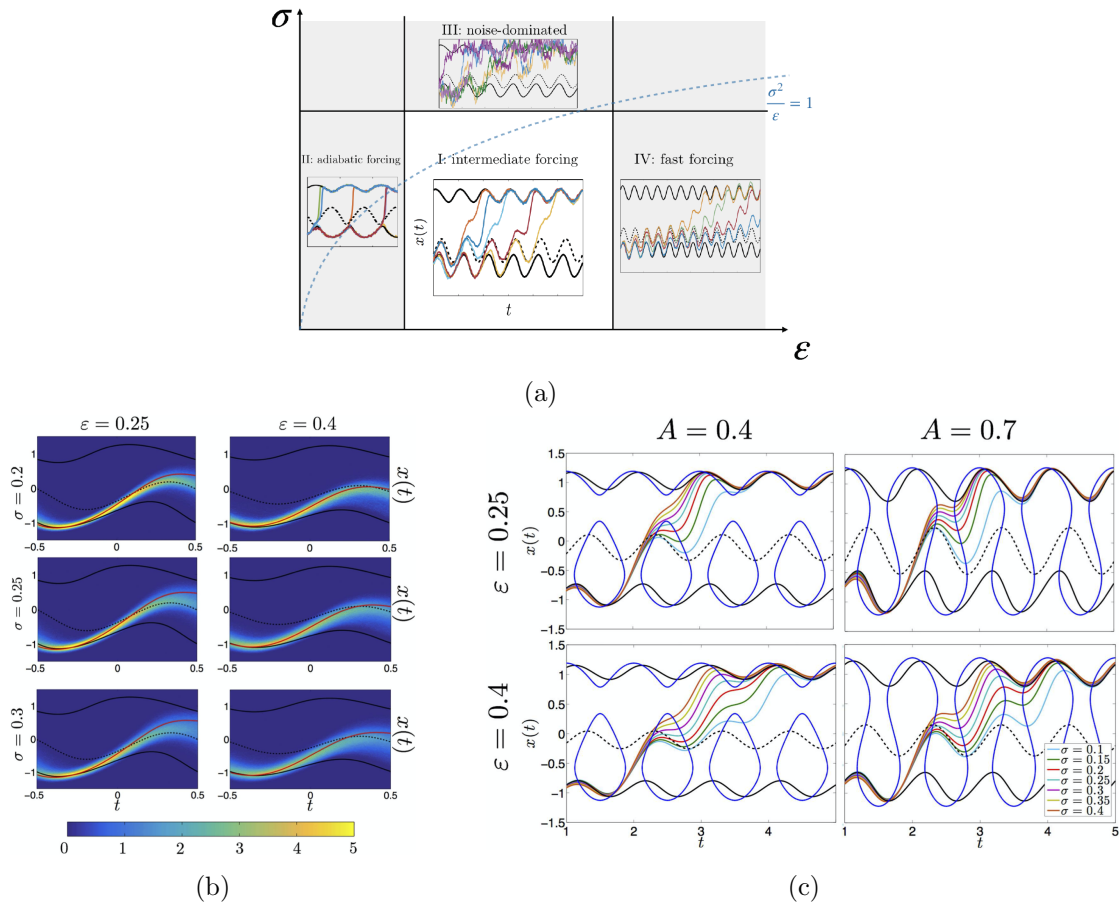

(a)

(b)

(c)

Figure 6: (a) Schematic (ε, σ)-parameter plane with inset figures depicting tipping realizations. Black solid (dashed) curves represent stable (unstable) solutions to the deterministic skeleton. (b) Comparison between most probable transition paths, represented by red curves, and Monte-Carlo simulations for $\alpha = 0.15$ and $A = 0.7$. (c) Summary of most probable transition paths. Nullclines of the deterministic skeleton are represented by blue curves and again black solid (dashed) curves represent stable (unstable) solutions.

To quantify tipping events from the lower limit cycle $x_l(t)$ to the upper one $x_u(t)$, we took a path

integral approach in which the most probable transition paths α^* are defined as minimizers of the Onsager-Machlup (OM) functional $I_\sigma : \mathcal{A} \mapsto \mathbb{R}$ defined by

$$I_\sigma[\alpha] = \int_{t_0}^{t_f} \left(\dot\alpha - \frac{1}{\varepsilon} f(\alpha, t) \right)^2 dt + \frac{\sigma^2}{\varepsilon} \int_{t_0}^{t_f} \frac{\partial f}{\partial x}(\alpha, t) dt, \tag{13}$$

where $\mathcal{A} = \{ \alpha \in H^1([t_0, t_f]; \mathbb{R}) : \alpha(t_0) = x_l(t_0), \alpha(t_f) = x_u(t_f) \}$ [55, 56]. This functional appears as the argument of an exponential function when formally constructing the probability density on $\mathcal{A}$ and consists of the standard Freidlin–Wentzell (FW) functional [57] with an additional term measuring the local expansion or compression of the vector field along a path $\alpha \in \mathcal{A}$. This additional term formally arises when using Girsanov's theorem to compute the Radon-Nikodym derivative of the Wiener measure with respect to the measure corresponding to the process generated by Eq.(12) [58, 59]. Typically, this additional term is discarded assuming $\sigma \ll 1$ and, using essentially a Γ-convergence argument, we were able to prove that the FW functional is indeed the limiting functional as $\sigma \to 0$ with ε fixed. However, the FW functional is not necessarily appropriate for this problem since minimizers are not unique – they can track the unstable limit cycle at no cost – and in the intermediate forcing regime σ^2/ε can be $O(1)$. Consequently, much of the work in [9] focused on studying what role the additional term in the OM functional plays in determining the most probable transition paths.

To compute minimizers of I_σ we implemented a gradient flow $\frac{\partial u}{\partial s} = -\frac{\delta I_\sigma}{\delta u}[u]$ with artificial time s. The stationary points of this gradient flow were compared with Monte-Carlo simulations of Eq.(12) and were in excellent agreement before crossing the unstable limit cycle; see Fig.6(b). In Fig.6(c), the most probable transitions paths were computed for various parameter values. The key observation from these results is that the transition from the lower to upper limit cycle is essentially independent of σ and occurs in a region in which the vector field is locally expansive. Heuristically, the bottlenecks through which the most probable transition path traverses can be understood as paths along which the integrand of I_σ is locally minimized; these occur when the nullcline intersects the lower limit cycle. Along the lower limit cycle, this result provides a deterministic indicator for regions in phase space in which the system is most susceptible to tipping.

2.5   Free boundary problems in polygonal domains

In [10], we studied a free boundary problem with a specific intent on analyzing the behavior of the free boundary near Neumann corner points. The specific free boundary problem we considered is variational with a corresponding functional $J : K \mapsto \mathbb{R}^+$ defined by

$$J[v] = \int_\Omega \left(|\nabla v|^2 + \lambda^2(v) \right) dx, \tag{14}$$

where $\Omega \subset \mathbb{R}^2$ is a bounded, convex domain and for $\lambda_1 > \lambda_2 > 0$ the function $\lambda : \mathbb{R} \mapsto \mathbb{R}^+$ is defined by

$$\lambda(v) = \begin{cases} \lambda_1, & v > 0 \\ \lambda_2, & v \le 0 \end{cases}.$$

The admissible set for this problem is defined by $K = \{ v \in H^1(\Omega) : v|_S = u_0 \}$ where $v_0 \in H^1(\overline{\Omega})$ and $S \subsetneq \Omega$. It can be shown by computing the variational derivative that minimizers of J satisfy the following conditions: (i) $\Delta u = 0$ on $\{u > 0\} \bigcup \{u < 0\}$, (ii) $u = u_0$ on S, (iii) the normal derivative satisfies $\frac{\partial u}{\partial \nu} = 0$ on $N = \partial\Omega \setminus S$, and (iv) on the free boundary $\Gamma = \partial\{u > 0\}$,

$$\left| \nabla u^+ \right|^2 - \left| \nabla u^- \right|^2 = \lambda_1^2 - \lambda_2^2, \tag{15}$$
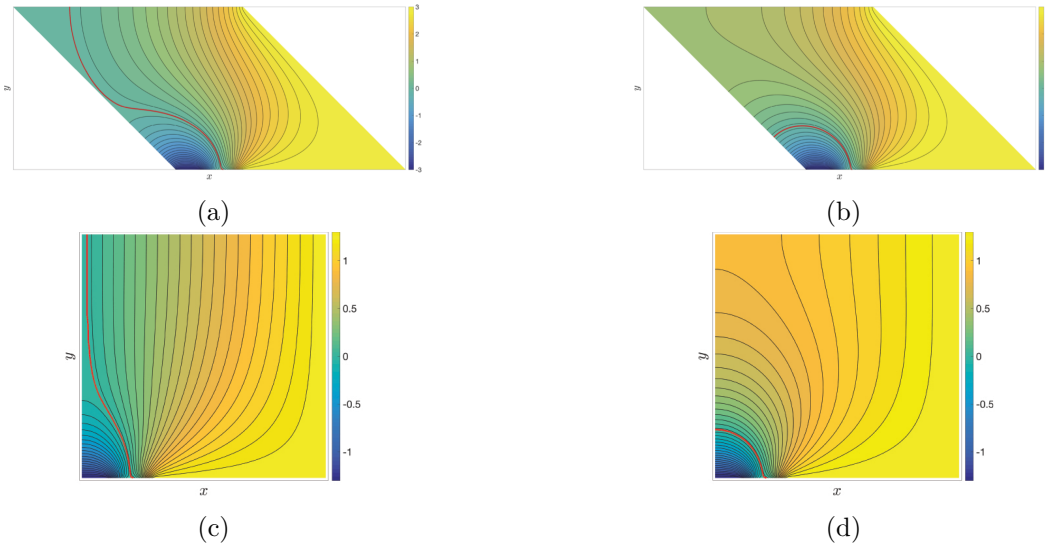
Figure 7: Contour plots of numerical solutions to the free boundary problem with the solid red curve corresponding to the numerical approximation of the free boundary. The upper left corner of each domain has Neumann boundary conditions on either side of the corner point. We illustrate the behavior of the minimizer when the free boundary lies to the right and left of the corner point for (a-b) acute angles and (c-d) right angles. In each case, the varying behavior of the free boundary was controlled by the Dirichlet boundary conditions on the bottom of the polygon.

where $u^+ = \max\{0, u\}$ and $u^- = \max\{0, -u\}$ [60]. In this derivation, the Neumann boundary conditions on N arise as 'natural boundary conditions' and the gradient jump condition results from the fact that the distributional derivative of $\lambda^2(v)$ is a delta function of mass $\lambda_1^2 - \lambda_2^2$.

The challenge with numerically solving this problem is that knowledge of the free boundary Γ is needed *a priori*. To ameliorate this problem, we defined a family of self similar transition layers $\phi_\varepsilon \in C^{1,1}(\mathbb{R}; [\lambda_1^2, \lambda_2^2])$ satisfying $\phi_\varepsilon = \phi_1(v/\varepsilon)$, $\phi_\varepsilon(v) \to \lambda^2(v)$ pointwise, $\phi_\varepsilon' \to (\lambda_2^2 - \lambda_1^2)\delta(v)$ in the sense of distributions, and we considered the relaxed functional $J_\varepsilon : K \mapsto \mathbb{R}^+$ defined by

$$J_\varepsilon[v] = \int_\Omega \left(|\nabla v|^2 + \phi_\varepsilon(v) \right) dx. \tag{16}$$

Using a Γ-convergence type argument, we proved that local minimizers of J_ε converge with respect to the strong topology in H^1 to minimizers of J and thus the zero level set of minimizers of J_ε well approximate the free boundary Γ. Finally, the minimizers of J_ε were numerically computed as the stationary points of the gradient flow $v_t = 2\Delta v - \phi_\epsilon'(v)$ with appropriate boundary conditions. Specifically, the numerical algorithm consisted of a standard centered finite difference scheme in space with ghost points to enforce the Neumann boundary conditions and an adaptive fourth order scheme in time. In Fig.7, the interaction of the numerically computed free boundary is illustrated for acute and right Neumann corner points; the obtuse case did not yield any nontrivial behavior. These numerical experiments indicate that the orthogonality condition resulting from the Neumann boundary conditions generates interesting behavior near acute or right angles. In particular, the free boundary, as it approaches a right angle, becomes tangent to the other side of the polygon and, as it traverses through the corner, travels a significant distance very quickly. On the other hand, as the free boundary approaches an acute corner point, there is a 'forbidden' region in which the free boundary does not enter due to the need for orthogonality and the energy constraints.

2.6   Noise-induced tipping in piecewise smooth systems:

Motivated by conceptual climate models with discontinuous vector fields, see for example [61–63], in [11] we developed a mathematical framework for determining most probable transition paths in stochastic differential equations with a piecewise smooth drift. Specifically, we considered a generic system of the form

$$d\mathbf{x}_t = \mathbf{F}(\mathbf{x}_t)dt + \sigma d\mathbf{W}_t, \tag{17}$$

where $\mathbf{x} = (x, \mathbf{y}) \in \mathbb{R}^n$, $x \in \mathbb{R}$, $\mathbf{y} \in \mathbb{R}^{n-1}$, $\sigma \in \mathbb{R}$, $\mathbf{W} = (W_1, \ldots W_n)$ is an n-dimensional Wiener process, and $\mathbf{F} : \mathbb{R}^n \setminus \{x = 0\} \mapsto \mathbb{R}^n$ is defined by

$$\mathbf{F}(\mathbf{x}) = \begin{cases} \mathbf{F}^+(\mathbf{x}), & x > 0 \\ \mathbf{F}^-(\mathbf{x}), & x < 0 \end{cases}. \tag{18}$$

For the deterministic skeleton, the dynamics in the regions $S_\pm = \{\mathbf{x} \in \mathbb{R}^n : \pm x > 0\}$ is clear while the dynamics on the switching manifold $\Sigma = \{\mathbf{x} \in \mathbb{R}^n : x = 0\}$ is not well defined and in many applications is typically imposed either through Fillipov's convex combination method [64–66] or through more sophisticated techniques [67–69]. A natural question is the role of noise in determining not only transition paths but also the dynamics near attracting (Σ_A) and repelling (Σ_R) subsets of Σ as well as crossing regions $\Sigma_\pm$ from S_+ to S_- and from S_- to S_+; see Fig.8 for a schematic diagram illustrating the possible dynamics near Σ.

<center>(a)   (b)   (c)</center>
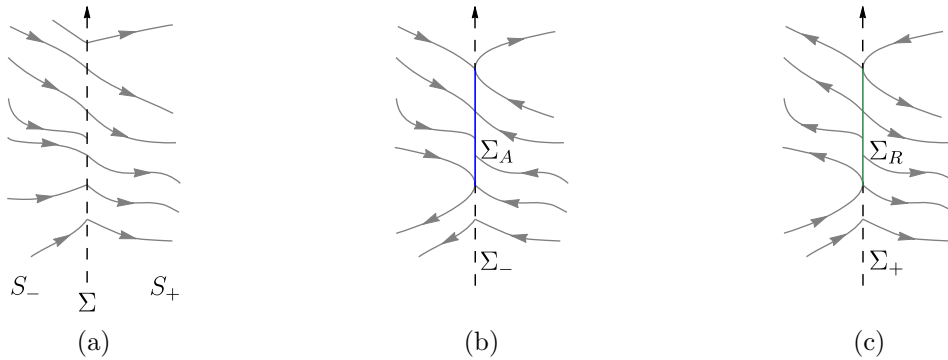
Figure 8: Generic phase planes illustrating possible behavior of the dynamical system near Σ. Depending on the normal component of the vector field on either side of Σ, subsets of Σ can be classified as (a) crossing, (b) attracting, or (c) repelling.

To address these questions, we took a path integral approach with a mollified version of the vector field and rigorously considered the convergence of minimizers of a rate functional as the width of the mollification parameter goes to zero. Specifically, for $\varepsilon > 0$ and $\mathbf{x}_0, \mathbf{x}_f \in \mathbb{R}^n$, we considered the sequence of Freidlin-Wentzell functionals $I_\varepsilon^{(t_0, t_f)} : \mathcal{A} \mapsto \mathbb{R}^+$ defined by

$$I_\varepsilon^{(t_0, t_f)}[\boldsymbol{\alpha}] = \int_{t_0}^{t_f} \left| \dot{\boldsymbol{\alpha}}(t) - \varepsilon^{-1}\zeta(\alpha(t)/\varepsilon) * \mathbf{F}(\boldsymbol{\alpha}(t)) \right|^2 dt, \tag{19}$$

where ζ is a smooth, unit area function compactly supported on $[-1, 1]$, $\mathcal{A} = \{\boldsymbol{\alpha} \in H^1([t_0, t_f]; \mathbb{R}^n) : \boldsymbol{\alpha}(t_0) = \mathbf{x}_0$ and $\boldsymbol{\alpha}(t_f) = \mathbf{x}_f\}$, and α denotes the first component of $\boldsymbol{\alpha}$. Assuming mild growth conditions on $\mathbf{F}$ as well asymptotically inward pointing flow, we used the direct method of calculus of variations to prove the existence of minimizers for this functional. Namely, by computing the Γ-limit of I_ε as $\epsilon \to 0$, we proved that minimizers of I_ε weakly converge in the H^1 topology to a minimum of

the functional $I : \mathcal{A} \mapsto \mathbb{R}^+$ defined by

$$I^{(t_0,t_f)}[\boldsymbol{\alpha}] = \int_{\mathcal{I}[\boldsymbol{\alpha}]} \|\dot{\boldsymbol{\alpha}}(t) - \mathbf{F}(\boldsymbol{\alpha}(t))\|^2 \, dt + \int_{\mathcal{I}_\Sigma[\boldsymbol{\alpha}]} \min_{\lambda \in [0,1]} \left\{ \left[\lambda F_1^+(0, \boldsymbol{\beta}(t)) + (1-\lambda) F_1^-(0, \boldsymbol{\beta}(t)) \right]^2 \right.$$
$$\left. + \left| \dot{\boldsymbol{\beta}} - \lambda \mathbf{G}^+(0, \boldsymbol{\beta}(t)) - (1-\lambda) \mathbf{G}^-(0, \boldsymbol{\beta}(t)) \right|^2 \right\} \, dt, \tag{20}$$

where we have decomposed the path and vector fields into components as $\boldsymbol{\alpha}(t) = (\alpha(t), \boldsymbol{\beta}(t))$, $\mathbf{F} = (F, \mathbf{G})$, and the intervals of time are defined by $\mathcal{I}[\boldsymbol{\alpha}] = \{t : \boldsymbol{\alpha}(t) \notin \Sigma\}$ and $\mathcal{I}_\Sigma[\boldsymbol{\alpha}] = \{t : \boldsymbol{\alpha}(t) \in \Sigma\}$. Not surprisingly, this functional consists of the standard Freidlin-Wentzell functional for times when $\boldsymbol{\alpha}(t) \in S_\pm$, but on Σ the drift is replaced by a nontrivial convex combination of $\mathbf{F}$. This result is interesting in that the limiting rate functional is independent of the chosen mollifier. Moreover, the most probable path may track the Filippov dynamics with no additional contribution on Σ_A and Σ_R. That is, on Σ_A and Σ_R, the minimizer of $I^{(t_0,t_f)}$ will satisfy $\dot{\boldsymbol{\beta}} = \lambda \mathbf{G}^+(0, \boldsymbol{\beta}(t) + (1-\lambda) \mathbf{G}^-(0, \boldsymbol{\beta}(t))$ with λ given by

$$\lambda(\boldsymbol{\beta}(t)) = \frac{F_1^-(0, \boldsymbol{\beta}(t))}{F_1^-(0, \boldsymbol{\beta}(t)) - F_1^+(0, \boldsymbol{\beta}(t))}, \tag{21}$$

which is precisely the definition of the Filippov convex combination. This result indicates, at least in applications in which the discontinuous vector field arises via approximation of a smooth vector field, the Filippov dynamics is the correct dynamics to impose on Σ.

We also demonstrated the utility of the derived rate functional through two case studies. The first consisted of a planar piecewise-linear system in which we could explore the interaction of most probable transition paths with Σ_A and Σ_R; see Fig.9(a-b). It is interesting to note for this case study, in the attracting, both the most probable transition path and the Monte-Carlo simulations track Σ_A. In contrast, in the repelling case, the most probable transition paths are not unique, but the Monte-Carlo simulations track a local minimum which does not slide along Σ_R. The second case study we considered was a one-dimensional periodically forced piecewise-linear system; see Fig.9(c-d). In this case study there was remarkable agreement between the Monte-Carlo simulations and the most probable transition path.
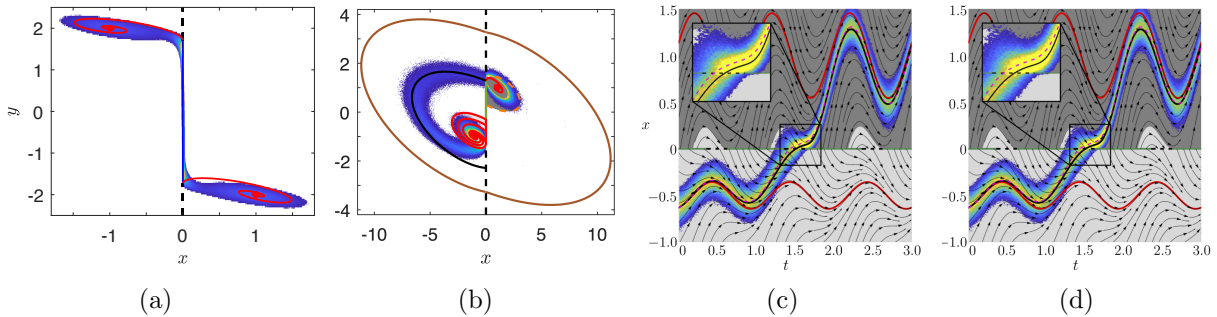

(a)   (b)   (c)   (d)

Figure 9: (a-b) Distribution of tipping events between fixed points for a piecewise-linear autonomous system compared with most probable paths (red and black curves) for parameter regimes in which (a) $\Sigma_A \neq \emptyset$ and (b) $\Sigma_R \neq \emptyset$. (c-d) Most probable transition paths (black curve) between limit cycles for a piecewise-linear one dimensional system with periodic forcing overlaid on the probability density generated by Monte-Carlo simulations (mean magenta curve). The dark (light) grey region corresponds to the basin of attraction for the upper (lower) limit cycle.

3   Ongoing and Future Research

Since the beginning of my mathematical career, my research has primarily focused on studying variational problems with multiple scales. In my ongoing research, I plan to continue this line of research with specific applications to noise-induced tipping in stochastic differential equations. I have also become interested in the study of dynamical systems on adaptive networks. Specifically, I am interested in the control of networks in which the individual nodes modify the topology of the network in response to the dynamics, e.g., spread of infectious diseases, spread of ideologies. I have found that my research interests tend to evolve into different application areas as my expertise grows, and it is difficult to predict in the long term, i.e., greater than five years, what areas of research I will pursue. However, in the following subsections I expand upon my immediate research plans.

3.1   Noise-induced tipping

As an extension of my work in [9, 11], I will continue developing a theory for understanding noise-induced transitions in stochastic differential equations (SDEs) with multiple scales. Specifically, I will focus on understanding most probable transition paths for SDEs on $\mathbb{R}^n$ conditioned to transition between states $\mathbf{x}_0$ and $\mathbf{x}_f$ over the interval of time $[t_0, t_f]$:

$$\begin{cases} d\mathbf{x} = \mathbf{F}(\mathbf{x})dt + \sigma dW_t \\ \mathbf{x}(t_0) = \mathbf{x}_0 \text{ and } \mathbf{x}(t_f) = \mathbf{x}_f \end{cases}, \tag{22}$$

where $\mathbf{F} : \mathbb{R}^n \mapsto \mathbb{R}^n$ is a smooth vector field, $\sigma > 0$, and W_t is standard n-dimensional Brownian motion. In this formulation, most probable transition paths $\alpha \in H^1([t_0, t_f]; \mathbb{R}^n)$ from state $\mathbf{x}_0$ to $\mathbf{x}_f$ are defined to be minimizers of a higher dimensional version of the Onsager-Machlup (OM) functional given by

$$I_\sigma[\alpha] = I_{\text{FW}}[\alpha] + \sigma^2 I_{\text{OM2}}[\alpha] = \int_{t_0}^{t_f} \|\dot{\alpha}(t) - \mathbf{F}(\alpha(t))\|^2 dt + \sigma^2 \int_{t_0}^{t_f} \nabla \cdot \mathbf{F}(\alpha(t)) dt. \tag{23}$$

As was discussed in Section 4 for the one dimensional case, this functional is the sum of the FW rate functional I_{FW} penalizing deviations of the path from the flow and an additional integral $\sigma^2 I_{\text{OM2}}$ measuring the total expansion or compression of the flow along a path. Ultimately, the competition between I_{FW} and $\sigma^2 I_{\text{OM2}}$ selects the optimal path, but formally the contribution of $\sigma^2 I_{\text{OM2}}$ is negligible in the small noise limit. In particular, if we let α_σ denote a sequence of minimizers for I_σ, then (up to a subsequence) it can be proved that there exists α_0 such that $\lim_{\sigma \to 0} \|\alpha_\sigma - \alpha_0\|_{H^1} = 0$ and α_0 minimizes I_{FW} [70]; that is, minimizers of I_σ are well approximated by minimizers of the FW functional in the vanishing noise limit. However, this argument for discarding the contribution of I_{OM2} may not hold when considering problems with additional small scale parameters. In the following research projects, I will study various problems in which the multiple scales in the problem are relevant and in which a rigorous theory needs to be developed to determine if the most probable transition paths can be completely described by minimizers of I_{FW} alone.

3.1.1   Most probable transitions for SDEs with piecewise-smooth drift

As a direction extension of [11], consider Eq.(22) with a discontinuous vector field of the following generic form:

$$\mathbf{F}(\mathbf{x}) = \begin{cases} \mathbf{F}^+(\mathbf{x}), & h(\mathbf{x}) > 0 \\ \mathbf{F}^-(\mathbf{x}), & h(\mathbf{x}) < 0 \end{cases}, \tag{24}$$

where $\mathbf{F}^\pm : \mathbb{R}^n \mapsto \mathbb{R}^n$ and $h : \mathbb{R}^n \mapsto \mathbb{R}$ are smooth and the so-called *switching manifold* $\Sigma = h^{-1}(0)$ is a smooth simply connected co-dimension one submanifold of $\mathbb{R}^n$. As in [11], if we let δ_ε be a delta

sequence and $\mathbf{F}_\varepsilon = \mathbf{F} * \delta_\varepsilon$ be a mollified version of $\mathbf{F}$, we obtain a smoothed out version of the OM functional given by

$$I_{\sigma,\varepsilon}[\alpha] = \int_{t_0}^{t_f} \|\dot\alpha(t) - \mathbf{F}_\varepsilon(\alpha(t))\|^2 dt + \sigma^2 \int_{t_0}^{t_f} \nabla \cdot \mathbf{F}_\varepsilon(\alpha(t)) dt. \tag{25}$$

The effect of this mollification is the discontinuity Σ is replaced by a mollified region of characteristic width ε centered on Σ. While the vector field $\mathbf{F}_\varepsilon$ is smooth in the mollified region, the directional derivatives of $\mathbf{F}_\varepsilon$ normal to Σ is unbounded in the limit $\varepsilon \to 0$. Due to the singular nature of this problem, there are a number of anticipated challenges that will arise in the analysis of this system which are as follows.

Challenge 1: This problem has two small parameters σ and ε, and if $\alpha_{\sigma,\varepsilon}^*$ denote minimizers of $I_{\sigma,\varepsilon}$, then, generically,

$$\lim_{\sigma\to0}\lim_{\varepsilon\to0} \alpha_{\sigma,\varepsilon} \neq \lim_{\varepsilon\to0}\lim_{\sigma\to0} \alpha_{\sigma,\varepsilon} \quad \text{and} \quad \lim_{\sigma\to0}\lim_{\varepsilon\to0} I_{\sigma,\varepsilon}[\alpha_{\sigma,\varepsilon}] \neq \lim_{\varepsilon\to0}\lim_{\sigma\to0} I_{\sigma,\varepsilon}[\alpha_{\sigma,\varepsilon}]. \tag{26}$$

In fact, from dimensional analysis, $\nabla \cdot F_\varepsilon$ scales like ε^{-1} and, thus there are different scaling regimes $\sigma^2 \ll \varepsilon$, $\sigma^2 \sim \varepsilon$, $\sigma^2 \gg \varepsilon$, and the behavior of minimizers is expected to be different in these scaling regimes.

Challenge 2: Given a sequence $\alpha_{\sigma,\varepsilon}$ of minimizers of $I_{\sigma,\varepsilon}$, it must be shown that any proposed limiting functional $I_{0,0}$ must satisfy the property that if $\alpha_{\sigma,\varepsilon}^*$ minimizes $I_{\sigma,\varepsilon}$ and $\alpha_{\sigma,\varepsilon}^* \to \alpha_{0,0}^*$ then $I_{\sigma,\varepsilon}[\alpha^*] \to I_{0,0}[\alpha_{0,0}^*]$.

Challenge 3: Different limiting functionals which arise in various asymptotic regimes could depend on the specific properties of the chosen δ_ε sequence, i.e., the smoothing. This would have practical implications for physical systems and, in particular, conceptual climate models.

Challenge 4: The distribution of tipping events for the SDE with discontinuous drift given by Eq.(24) should concentrate around minimizers of the limiting functional. Again, this could depend on the δ-sequence chosen.

A natural starting point to address the above issues is to consider the scaling $\varepsilon = \sigma^p$, where $p > 0$, and study the convergence of minimizers of the functional I_{σ,σ^p} using Γ-convergence. Recall, we say I_{σ,σ^p} Γ-converges to I_0^p if the following properties are satisfied [71, 72]:

1. **Liminf inequality:** For all sequences of curves $\alpha_\sigma \in H^1([t_0, t_f]; \mathbb{R}^n)$ satisfying $\alpha_\sigma \to \alpha_0$,

$$I_0^p[\alpha_0] \leq \liminf_{\sigma\to0} I_{\sigma,\sigma^p}[\alpha_\sigma].$$

2. **Recovery sequence:** For all α_0 there exists a sequence $\alpha_\sigma \in H^1([t_0, t_f]; \mathbb{R}^n)$ such that $\alpha_\sigma \to \alpha_0$ and

$$I_0^p[\alpha_0] = \lim_{\sigma\to0} I_{\sigma,\sigma^p}[\alpha_p].$$

These two conditions ensure that I_{σ,σ^p} has a common lower bound, the lower bound is optimal, and that the limiting functional is precisely this lower bound. Note that in this definition there is no mention of either the type of convergence, e.g., strong or weak, nor the function space α_0 is defined on. This is intentional since, in proving a Γ-limit, some notion of compactness is needed and thus it is necessary to often work in the weak topology. Moreover, α_0 may lie in a space with lower regularity.

The Γ-limit is the natural notion of a limiting functional in the sense that under the mild condition of equi-coercivity of I_{σ,σ^p}, if α_0^* minimizes I_0^p then there exists a sequence α_σ^* that minimizes I_{σ,σ^p} and satisfies $\alpha_\sigma^* \to \alpha_0^*$ [71, 72]. That is, the asymptotic limit points of I_{σ,σ^p} are exactly the minimizers of I_0^p. However, one of the challenges with proving a Γ-limit is that the target limiting functional must be formed from an educated guess based on an analysis of minimizers. In the system of interest, it is natural to expect that the appropriate Γ-limit will correspond to the standard FW functional except for intervals of time on which the curve tracks Σ. This motivates the following tasks.

Task 1: Construction of a recovery sequence.   To construct a recovery sequence for a given curve α_0 it is necessary to calculate the optimal transition through the mollified region. If we introduce the conjugate momentum $\varphi = \dot{\alpha} - \mathbf{F}_\varepsilon(\alpha)$, it follows that in the mollified region minimizers of $I_{\sigma,\varepsilon}$ satisfy the following system of equations [57, 73]:

$$\begin{cases} \dot{\alpha} = \varphi + \mathbf{F}_\varepsilon(\alpha) \\ \dot{\varphi} = -\nabla\mathbf{F}_\varepsilon(\alpha)\varphi + \sigma^2\nabla(\nabla \cdot \mathbf{F}_\varepsilon(\alpha)) \end{cases} . \tag{27}$$

Since spatial derivatives of $\mathbf{F}$ scale like $\varepsilon^{-1} = \sigma^{-p}$ in the mollified region, this system can be interpreted as a fast-slow system. This observation allows the use of geometric singular perturbation theory to compute the optimal transition [74]. Specifically, in the mollified region, the optimal transition will predominantly track the flow on the slow manifold, if it exists, after an initial short transient time spent on a fast fiber. However, scaling arguments indicate the structure of the slow manifold will depend on the value of p and in particular the slow manifolds are given approximately by the following locus of points in phase space: $0 = \nabla(\delta_1 * \mathbf{F}(\mathbf{x}))\varphi - \nabla(\nabla \cdot \delta_1 * \mathbf{F}(\mathbf{x}))$ if $p = 2$, i.e., $\sigma^2 \sim \varepsilon$; $0 = \nabla(\delta_1 * \mathbf{F}(\mathbf{x}))\varphi$ if $p < 2$, i.e., $\sigma^2 \ll \varepsilon$; and $0 = \nabla(\nabla \cdot \delta_1 * \mathbf{F}_\varepsilon(\mathbf{x}))$ if $p > 2$, i.e., $\sigma^2 \gg \varepsilon$. Regardless of the scaling regime, the recovery sequence will transition through the mollified region along a fast fiber or by a path restricted to the slow manifold.

Task 2: Computation of limiting rate functional.   The explicit form of the limiting functional will depend on the value of the functional computed along the recovery sequence. The computation of the most probable path means optimizing the rate functional over the transition paths on the slow manifold in the mollified region. This computation is simplified by the fact that Eq.(27) is a Hamiltonian system with Hamiltonian $H(\mathbf{x}, \varphi) = \frac{1}{2}\langle\varphi, \varphi\rangle + \langle\mathbf{F}_\varepsilon(\mathbf{x}), \varphi\rangle - \sigma^2\nabla \cdot \mathbf{F}_\varepsilon(\mathbf{x})$ through which the Lagrangian is related via a Legendre transformation. The fact that this system is Hamiltonian implies that the optimal paths are further restricted to flowing on surfaces on which the Hamiltonian is constant. In the special case in which the transition path is between fixed points, this implies the optimal path will be a heteroclinic orbit of the Hamiltonian system. These facts will allow us to exploit the Hamiltonian structure to compute the rate functional along optimal transitions on the slow manifolds in the various scaling regimes.

Task 3: Liminf inequality.   The challenge with rigorously proving the liminf inequality is to show that the recovery sequence is optimal. This work involves using functional analytic tools, namely weak convergence and Sobolev embedding theorems, to rigorously prove the optimal lower bound, an area in which I have previous experience [1, 2, 7, 10, 11].

The above tasks will address the first two challenges and form one area of my main mathematical research. However, the third and fourth challenges are more nuanced and problem specific but are more appropriate research problems for undergraduate and master's students to tackle. Specifically, in low dimensional models these questions can be addressed, at least numerically, in a case by case manner and provide an excellent source of problems in which both undergraduate and master's students can

contribute. Indeed, I am currently mentoring Grace Hofmann (Master's student, Wake Forest) on a project studying a piecewise smooth version of the Wilson-Cowan equations [75].

3.2   Most probable transition paths for SDEs with non-autonomous drift

Consider Eq. (22) with a time dependent parameter:

$$\begin{cases} d\mathbf{x} = \mathbf{F}(\mathbf{x}; \Lambda(t))dt + \sigma dW_t \\ \mathbf{x}(t_0) = \mathbf{x}_0 \text{ and } \mathbf{x}(t_f) = \mathbf{x}_f \end{cases}, \tag{28}$$

where $\Lambda : \mathbb{R} \mapsto \mathbb{R}$ is a smooth monotone increasing function that is asymptotically constant, i.e., there exists $\Lambda_{\pm} \in \mathbb{R}$ such that $\lim_{\to \pm\infty} \Lambda(t) = \Lambda_{\pm}$. In climate applications, the function Λ is often called a ramp and is a proxy for anthropogenic effects that cause sudden rapid transitions between the parameter values $\Lambda_{\pm}$. In the absence of noise, the sudden transition between stable states for the dynamics of Eq.(28) in response to Λ is the central study of rate induced tipping [76–81]. The challenge with adapting the FW theory of large deviations directly to Eq.(28) is that rigorous results concerning the concentration of tipping events around minimizers of I_{σ} only hold in autonomous systems [57]. There are some exceptions to this statement, specifically in periodically forced systems with slow forcing [47–51, 82–85] and periodically forced systems with small noise [9, 54, 86–90], but these studies rely on the system being one dimensional and the complication that the system is non-autonomous is effectively removed by considering the problem in a cylindrical phase space.

The approach I will take to study this problem is to rewrite the system as an autonomous system by exploiting the structure of the ramp:

$$\begin{cases} d\mathbf{x} = \mathbf{F}(\mathbf{x}; r)dt + \sigma_1 dW_t \\ dr = \Lambda'(\Lambda^{-1}(r))dt + \sigma_2 dW_t \\ \mathbf{x}(t_0) = \mathbf{x}_0 \text{ and } \mathbf{x}(t_f) = \mathbf{x}_f \\ r(t_0) = \Lambda_- \text{ and } r(t_f) = \Lambda_+ \end{cases}. \tag{29}$$

Note that the deterministic skeleton of this system is autonomous with fixed points satisfying the equation $\mathbf{F}(\mathbf{x}; \lambda_{\pm}) = 0$. That is, the non-autonomous part of the system has been 'compactified' in the sense that compact invariant sets such as equilibria now describe the long time behavior of the system. The process of compactification described above is not restricted to ramp functions but is more broadly applicable to other forms of non-autonmous forcing [91]. Assuming $\sigma_1, \sigma_2 \ll 1$, the contribution from $\sigma^2 I_{OM2}$ is negligible and thus the FW functional corresponding to Eq.(29) can be expressed in the form:

$$I_{\sigma_1,\sigma_2}[\alpha, \beta] = \frac{I_1[\alpha, \beta]}{\sigma_1^2} + \frac{I_2[\alpha]}{\sigma_2^2} = \int_{t_0}^{t_f} \frac{\|\dot{\alpha} - \mathbf{F}(\alpha; \beta)\|^2}{\sigma_1^2}dt + \int_{t_0}^{t_f} \frac{|\dot{\beta} - \Lambda'(\Lambda^{-1}(\beta))|^2}{\sigma_2^2}dt, \tag{30}$$

where the path the ramp takes is a curve $\beta : [t_0, t_f] \mapsto \mathbb{R}$ satisfying $\beta(t_0) = \Lambda_-$ and $\beta(t_f) = \Lambda_+$. This is again a variational problem with multiple scales and the following challenges are anticipated in its analysis.

Challenge 5:   As in Chalenges 1-2, we expect minimizers will have different behaviors in different scaling regimes, i.e., $\sigma_2 \ll \sigma_1$, $\sigma_2 \sim \sigma_1$, and $\sigma_1 \ll \sigma_2$. Each of these regimes has different physical import and correspond to weak noise on the ramp, balanced noise between the drift and the ramp, and weak noise on the drift, respectively. Again, to compute a Γ-limit a single small parameter is introduced by defining $\sigma_2 = \sigma_1^p$ for some $p > 0$.

Challenge 6:   There is a third potential small scale parameter in I_{σ_1,σ_2}, namely the characteristic time scale on which the ramp transitions between states defined by $\tau = (\|\Lambda'\|_\infty)^{-1}$. The scaling regions discussed in challenge 5 implicitly assumed that $\sigma_1, \sigma_2 \ll \tau$ and $\tau = O(1)$. However, for very fast tipping, i.e., $\tau \ll 1$, there are nine additional parameter regimes of interest: $\sigma_1 \sim \tau \ll \sigma_2$, $\sigma_2 \ll \sigma_1 \sim \tau_1$, $\sigma_2 \sim \tau \ll \sigma_1$, $\sigma_1 \ll \tau \sim \sigma_2$, $\sigma_1 \ll \tau \ll \sigma_2$, $\sigma_2 \ll \tau \ll \sigma_1$, $\sigma_1 \ll \tau \ll \sigma_1$, $\sigma_2 \ll \tau \ll \sigma_1$, and $\tau \ll \sigma_1 \sim \sigma_2$.

Task 4: Optimal paths in the regime $\sigma_2 \ll \sigma_1$.   In this scaling regime we expect that optimal paths will consist of minimizing the first term in the integrand of I_{σ_1,σ_2} subject to the constraint $\dot{\beta} = \Lambda'(\Lambda^{-1}(\beta))$, i.e the time dependant parameter exactly follows the ramp. Again, the Γ-limit provides a natural technique for proving such a result. Note, I am familiar with the techniques needed to prove such a Γ-limit as they arise in elasticity theory when considering an isometry constraint [1–4].

Task 5: Optimal paths in the regime $\sigma_1 \ll \sigma_2$.   In this scaling regime the first term in the integrand of I_{σ_1,σ_2} dominates. However, in contrast with Task 4, optimal paths cannot satisfy the constraint $\dot{\alpha}(t) = \mathbf{F}(\alpha; \beta)$ and undergo tipping as this equation is only satisfied if the path follows the deterministic dynamics. Nonetheless, the divergence of $\sigma_1^{-2} I_1$ can be ameliorated by considering the scaled functional $\sigma_1^2 I_{\sigma_1,\sigma_2} = I_1 + \sigma_1^2 \sigma_2^{-2} I_2$ which provides the correct framework for proving a Γ-limit. In the Γ-limit, we expect that the contribution $\sigma_1^2 \sigma_2^{-2} I_2[\beta]$ will be negligible and thus, in some sense, the ramp β can be chosen arbitrarily. In particular, the optimal ramp can be abstractly considered as an optimal control selected so that the vector field $\mathbf{F}(\cdot; \beta)$ allows α to tip while at the same time tracking the flow as closely as possible.

Task 6: Optimal paths in the regime $\sigma_2 \sim \sigma_2$.   In this scaling regime there is no natural notion of a Γ-limit since both $\sigma_1^{-2} I_1$ and $\sigma_2^{-2} I_2$ are comparable. While in Tasks 4-5 I am proposing a unified theory, in this scaling regime the analysis is problem specific. However, in low dimensional dynamical systems, the optimal paths in this regime can be computed numerically through a gradient descent algorithm and compared with Monte-Carlo simulations. This type of analysis will be applicable in conceptual climate models in which the uncertainty in the ramp parameter and the underlying vector field are equivalent.

Task 7: Optimal paths in the regime $\tau \ll 1$.   To study the nine different scaling regimes a single small scale parameter must be introduced, e.g., $\sigma_2 = \sigma_1^p$, $\tau = \sigma_1^q$, and the appropriate Γ-limits must be computed. However, since τ will appear as a prefactor in front of Λ' in I_{σ_1,σ_2} and not on the highest order derivatives, we can use information from the Γ-limits in Task 6 to simplify the analysis in some of these nine regimes. More precisely, the Γ-limits computed in Task 6 are stable under perturbations in the sense that they are continuous with respect to strong convergence in H^1 [71,72]. Consequently, the various Γ-limits in these nine scaling regimes can be computed as further Γ-limits of the functionals computed in Task 6.

The above tasks are challenging and will form another branch of my main mathematical research. However, again in low dimensional systems, this area of research is ammenable to master's and PhD students. Indeed, I am currently collaborating with Katherine Slyman (PhD student, UNC Chapel Hill) and Nicholas Corak (PhD student, Wake Forest University) on two projects applying these techniques to a simple model of hurricane formation [92] and the El-Nino Southern Oscillation [93].
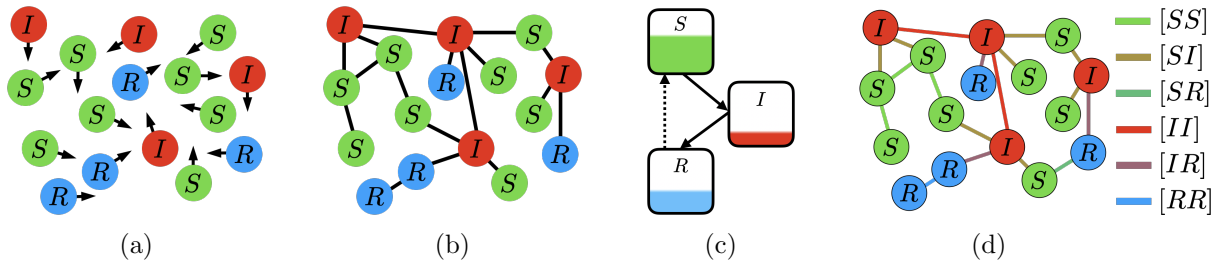
Figure 10: Illustration of mathematical frameworks for modeling the spread of infections diseases. (a) Agent based model coupling spatial dynamics with the spread of the disease. (b) Static network with the spread of the disease propagating along edges. (c) Compartment model with the disease spreading between the various population densities. (d) Adaptive network in which the population and edge densities are incorporated into compartment models.

3.3 Dynamics on adaptive networks

There are a large number of mathematical models for the spread of infectious diseases whose efficacy and validity vary over a wide range of spatial and temporal scales. Specifically, adapting terminology from condensed matter physics, typical mathematical models range from agent based models at the microscale [94], network models at the mesoscale [95, 96], and finally to mean-field compartment models at the macroscale [97–101]; see Figure 10(a-c). Following the pioneering of Kermack and McKendrick [102], the unifying thread in all of these models is that members of the population are categorized depending on their status, e.g.,, susceptible (S), infected (I), and recovered (R), and the dynamic evolution of each individual status is modeled either as a stochastic or purely deterministic process. The benefit of adopting a particular modeling framework ranges from the ability to simulate every minute detail of the disease at the agent based level to analyzing a small system of ordinary or partial differential equations at the compartment model level. In particular, compartmental models are particularly amenable to mathematical analysis as standard tools from dynamical systems can be used to categorize underlying mechanisms which dictate the qualitative behavior of the spread of the disease. Moreover, standard compartmental models such as the SIR model can be used as scaffolding onto which additional compartments can be added, e.g.,, exposed (E), vaccinated (V), hospitalized (H). However, while compartment models are useful predictive tools on a short timescale, on longer timescales classical models are unable to capture several realistic phenomenon such as multiple waves of infections and the feedback between human behavior and the spread of the disease. Moreover, it is difficult to incorporate non-pharmaceutical interventions such as sheltering in place, testing, and contact tracing into standard compartment models. Finally, in the analysis of many epidemiological models, there is an overemphasis on the ability of the basic reproduction number R_0 to predict the severity of a disease.

To address some of these questions, during the 2021-2022 academic year, and in collaboration with Hwayeon Ryu (Elon University), I was funded by a NSF Center for Undergraduate Research in Mathematics (CURM) minigrant to form a team of students in order to study the control of infectious diseases on adaptive networks. This collaboration was a direct follow up to my student's work in [13] as well as some projects I was involved in as part of a summer school I co-led[1]. The approach we took was to develop and analyze a hybrid model which bridges network models (mesocale) with ODE models (macroscale) and implement an optimal control strategy to minimize the economic impact as well as the spread of the disease.

As an example of how edge and population densities can be modeled as a system of ODEs, consider the classic SIR model with the edge density state variables $[SS]$, $[SI]$, $[SR]$, $[II]$, $[IR]$, and $[RR]$

---

[1]https://sinews.siam.org/Details-Page/virtual-summer-schools-can-we-make-them-work

introduced yielding the following system of differential equations:

$$\frac{d[S]}{dt} = -\frac{\beta}{N}[SI],$$

$$\frac{d[SI]}{dt} = \frac{\beta}{N}\left([SSI] - [ISI]\right) - \alpha[IS],$$

$$\frac{d[I]}{dt} = \frac{\beta}{N}[SI] - \alpha[I],$$

$$\frac{d[SR]}{dt} = -\frac{\beta}{N}[RSI] + \alpha[IS],$$

$$\frac{d[R]}{dt} = \alpha[I],$$

$$\frac{d[II]}{dt} = \frac{\beta}{N}\left([IS] + [ISI]\right) - 2\alpha[II],$$

$$\frac{d[SS]}{dt} = -\frac{\beta}{N}[SSI],$$

$$\frac{d[IR]}{dt} = \frac{\beta}{N}[RSI] + \alpha\left(2[II] - [IR]\right),$$

$$\frac{d[RR]}{dt} = \alpha[IR],$$

$$(31)$$

where $[ABC]$ denotes the average number of triplets with a given sequence of states $A, B, C \in \{S, I, R\}$; see Figure 10(d) for an illustration of a network with these state variables. The first three equations in this model are the standard SIR equations while the remaining equations correspond to the conversion of various edge types as nodes are infected or recover. This system of equations is often closed by using a counting argument to approximate the number of triple links by

$$[ABC] = \frac{q}{k}\frac{[AB][BC]}{[B]}, \qquad (32)$$

where k is the average degree of the nodes and q is the mean excess degree [96]. The approach of introducing edge densities as state variables has been used to model the spread of a disease on a network in which edges can rewire or delete edges in response to not only the state of the disease but the topology of the network [103]. The benefit of this framework is that hybrid models can exhibit a range of phenomenon such as periodic oscillations [95] and hysteresis [104–106] which are absent in standard compartment models.

In our work, we developed and analyzed an ODE system that in addition to modeling the dynamics of the relevant population densities also modeled the temporal evolution of the edge densities in the network. Specifically, we allowed for the pausing of edges in response to the spread of the disease to mimic sheltering in place and treated the pausing rate as a control. While we were able to address some of our initial questions, numerous further questions arose out of this work such as:

- How do we best implement pausing of a network in order to minimize spread of the disease while maximizing the economic output of the network?

- How should contact tracing be modeled given that such a process would necessarily look beyond direct connections, i.e., edges?

- How do we account for changes in the topology of the network as pausing is implemented?

While my work with students this past year has been fruitful, to address these questions there are a number of further challenges and tasks that have arisen out of our work that will be part of the focus of my ongoing research.

Challenge 7: The approximation for $[ABC]$ given in (32) assumes a homogeneous static network containing no triangles; see Fig.11(a). In the case of an adaptive network, a time varying moment closure is necessary to account for the change in the topology of the network. Moreover, such a moment closure must account for more sophisticated measures of the topology of the network, e.g., the clustering coefficient.
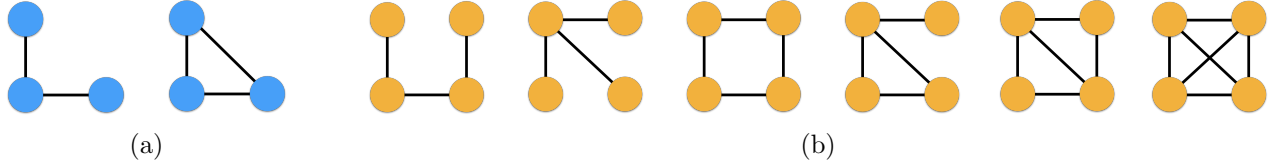
(a)   (b)

Figure 11: Illustration of possible topologically equivalent ways that (a) three and (b) four nodes could be connected in an undirected network.

Challenge 8:   The excess degree which arises in the moment closure is typically approximated by $q = k - 1$. However, we know from the "friendship paradox", i.e., your friends have on average more friends than you, that $q \geq k - 1$ and depends on the structure of the network [107]. This seemingly paradoxical statement arises from the fact that, when computing the expectation, selecting a node is drawn from a uniform distribution, while the selection of a non-adjacent connected node is drawn from a different distribution. Moreover, q will also be time dependent in adaptive networks.

Challenge 9:   In applications in which contact tracing is implemented, it is necessary to derive governing equations for triple links which will in turn require moment closure approximations for the quad links of which there are six possible topologically equivalent types [108]; see Fig.11(b). Again, with adaptive networks such moment closures will necessarily be time dependent.

Challenge 10:   In order to determine optimal control strategies for the types of models incorporating edge dynamics discussed above, a high dimensional system of differential-algebraic boundary value problems must be solved. For example, it follows from Pontryagin's maximum principle that if we wished to control Eq.(31) with a single control function then a system of 18 differential equations and one algebraic equation would have to be solved for the state, costate, and control.

Task 8: Derivation of governing equations from mean field approximation.   To address aspects of Challenge of 8 and 9, it is necessary to derive the hybrid differential equations directly from the Markov chain models which operate at the mesoscale. That is, Markov chain models typically begin by defining a status for each node, e.g., S, I, R, and a transition probability $P_{AB}(\Delta t)$ for a node to change status from A to B in an interval of time $\Delta t > 0$. Typically, P_{AB} scales like Δt and depends on the status of nearest neighbors if it is an infection probability or an intrinsic timescale if it is a probability corresponding to recovery. The mean field approximations are then derived by computing the expected value for the number of nodes of a certain status and considering the limit $\Delta t \to 0$ to obtain a system of ODEs [109,110]. For an adaptive network, it is further necessary to define transition probabilities for the entries of the adjacency matrix of the network itself, and thus when computing mean field approximations, additional state variables will need to be introduced to form a closed system of ODEs. For example, assuming a moment closure approximation of the form $[SI] = \overline{k}[S][I]$ and assuming pausing and reconnecting of edges is proportional to the number of infected nodes, we obtain the following version of Eq.(31) in the mean field limit

$$[\dot{S}] = \frac{\beta \overline{k}}{N}[S][I],$$

$$[\dot{I}] = \frac{\beta \overline{k}}{N}[S][I] - \alpha[I], \tag{33}$$

$$\dot{\overline{k}} = \eta(N - [I])(k - \overline{k}) - w[I]\overline{k},$$

where $k, \overline{k}$ are the average degrees of the static and adaptive network respectively, and $\eta, w > 0$. Note that this is essentially the standard SIR model with an additional equation for the temporal evolution

of the average degree. The weakness with this derivation is that the moment closure $[SI] = \overline{k}[S][I]$ assumes a fully connected network and given that the topology of the network is changing, a more realistic model should use more precise moment closure approximations. The task is then to derive governing equations for quantities such as k, q, and the clustering coefficient ϕ (see Task 9) which arise in higher order moment closures. This work will require careful analysis of the expected value computed from the transition probabilities.

Task 9: Derivation and implementation of moment closure approximations for time varying topologies. To address aspects of Challenges 7-9, it is necessary to consider the temporal evolution and validity of the moment closure approximation given by Eq.(32) which assumes that all connections are linear; see left diagram in Fig.11(a). For a network with adjacency matrix A, the clustering coefficient defined by

$$\phi = \frac{\mathrm{Tr}(A^3)}{\sum_{i,j}(A^2)_{ij} - \mathrm{Tr}(A^2)},\tag{34}$$

measures the ratio of the the number of triangles in a network to the number of linear triple links and one proposed moment closure that accounts for triangles is given by

$$[ABC] = \frac{q}{k}\frac{[AB][BC]}{[B]}\left((1-\phi) + \phi\frac{k[B][C][AC]}{([BB][C] + [B][CC])[A][BC]}\right).\tag{35}$$

This moment closure approximation is derived by separately computing the moment closure approximations for a network with no triangles and one consisting entirely of triangles and considering their convex combination with ϕ the weighting parameter [111]. To address Challenge 9, it is necessary to derive similar moment closure approximations for the six possible topologically equivalent ways that four nodes can be connected; see Fig.11, and compute the appropriate convex combination of these approximations. Moreover, connected with Task 8, ODEs must be derived for the temporal evolution of the weights arising in this combination.

Task 10: Implementation of optimal controls. In conjunction with Tasks 9 and 10, optimal control strategies will be implemented on the resulting systems. Specifically, we will consider minimizing a functional consisting of the cost of treatment of a disease and the economic output of the network. As discussed in Challenge 10, using the Pontryagin maximum for a generic cost functional will result in an intractable system for which it is not clear what can be concretely deduced regarding optimal policies beyond what is learned from the results of specific numerical simulations. As a starting point we will work with a functional that is linear in the cost of treatment as well as the labor, i.e., proportional to number of infected nodes and the number of edges. This structure of the functional will allow for the use of bang-bang controls, i.e., piecewise constant functions, for which direct analysis will be simplified.

These tasks will form the final branch of my immediate research goals. This area of research is also particularly amenable to collaboration with undergraduate students. Indeed, two of my former undergraduate students Minato Hiraoka (beginning PhD student at Northwestern University) and Sarah Ruth Nicholls (beginning PhD student at Rice University) as well as Malindi Whyte (rising senior) have contributed to aspects of this research. Specifically, they worked on a project studying optimal control of a simple SIS disease that will lead to a publication and their work has motivated much of the more nuanced challenges/tasks that I will pursue.

References

[1] J. A. Gemmer and S. C. Venkataramani, "Shape selection in non-Euclidean plates," *Physica D: Nonlinear Phenomena*, vol. 240, no. 19, pp. 1536–1552, 2011.

[2] J. Gemmer and S. Venkataramani, "Defects and boundary layers in non-Euclidean plates," *Nonlinearity*, vol. 25, no. 12, p. 3553, 2012.

[3] J. Gemmer and S. C. Venkataramani, "Shape transitions in hyperbolic non-Euclidean plates," *Soft Matter*, vol. 9, no. 34, pp. 8151–8161, 2013.

[4] J. Gemmer, E. Sharon, T. Shearman, and S. C. Venkataramani, "Isometric immersions, energy minimization and self-similar buckling in non-Euclidean elastic sheets," *EPL (Europhysics Letters)*, vol. 114, no. 2, p. 24003, 2016.

[5] K. K. Yamamoto, T. L. Shearman, E. J. Struckmeyer, J. A. Gemmer, and S. C. Venkataramani, "Nature's forms are frilly, flexible, and functional," *The European Physical Journal E*, vol. 44, no. 7, pp. 1–18, 2021.

[6] C. G. Durfee, J. Gemmer, and J. V. Moloney, "Phase-only shaping algorithm for Gaussian-apodized bessel beams," *Optics express*, vol. 21, no. 13, pp. 15777–15786, 2013.

[7] J. A. Gemmer, S. C. Venkataramani, C. G. Durfee, and J. V. Moloney, "Optical beam shaping and diffraction free waves: a variational approach," *Physica D: Nonlinear Phenomena*, vol. 283, pp. 15–28, 2014.

[8] S. Sabbah, J. Gemmer, A. Bhatia-Lin, G. Manoff, G. Castro, J. Siegel, N. Jeffery, and D. Berson, "A retinal code for motion along the gravitational and body axes," *Nature*, vol. 546, no. 7659, p. 492, 2017.

[9] Y. Chen, J. Gemmer, M. Silber, and A. Volkening, "Noise-induced tipping under periodic forcing: Preferred tipping phase in a non-adiabatic forcing regime," *Chaos: An Interdisciplinary Journal of Nonlinear Science*, vol. 29, no. 4, p. 043119, 2019.

[10] J. Gemmer, G. Moon, and S. Raynor, "Solutions to a two-dimensional, Neumann free boundary problem," *Applicable Analysis*, vol. 99, no. 2, pp. 214–231, 2020.

[11] K. Hill, J. Zanetell, and J. A. Gemmer, "Most probable transition paths in piecewise-smooth stochastic differential equations," *Physica D: Nonlinear Phenomena*, p. 133424, 2022.

[12] C. Grimm and J. A. Gemmer, "Weak and strong solutions to the inverse-square brachistochrone problem on circular and annular domains," *Involve, a Journal of Mathematics*, vol. 10, no. 5, pp. 833–856, 2017.

[13] H. Scanlon and J. Gemmer, "Epidemic conditions with temporary link deactivation on a network SIR disease model," *Spora: A Journal of Biomathematics*, vol. 7, no. 1, pp. 72–85, 2021.

[14] E. Efrati, E. Sharon, and R. Kupferman, "Elastic theory of unconstrained non-Euclidean plates," *Journal of the Mechanics and Physics of Solids*, vol. 57, no. 4, pp. 762–775, 2009.

[15] E. Sharon and E. Efrati, "The mechanics of non-Euclidean plates," *Soft Matter*, vol. 6, no. 22, pp. 5693–5704, 2010.

[16] M. Lewicka and L. Mahadevan, "Geometry, analysis, and morphogenesis: Problems and prospects," *Bulletin of the American Mathematical Society*, 2022.

[17] Y. C. Fung, *Foundations of solid mechanics*. Englewood Cliffs, N.J.: Prentice-Hall, 1965.

[18] M. Lewicka, L. Mahadevan, and M. R. Pakzad, "The Föppl-von Kármán equations for plates with incompatible strains," *Proceedings of the Royal Society A: Mathematical, Physical and Engineering Science*, vol. 467, no. 2126, pp. 402–426, 2011.

[19] M. Lewicka and M. Reza Pakzad, "Scaling laws for non-Euclidean plates and the $W^{2,2}$ isometric immersions of Riemannian metrics," *ESAIM: Control, Optimisation and Calculus of Variations*, vol. 17, no. 04, pp. 1158–1173, 2011.

[20] N. V. Efimov, "Generation of singularites on surfaces of negative curvature," *Matematicheskii Sbornik*, vol. 106, no. 2, pp. 286–320, 1964.

[21] M.-H. Amsler, "Des surfaces à courbure négative constante dans l'espace à trois dimensions et de leurs singularités," *Mathematische Annalen*, vol. 130, no. 3, pp. 234–256, 1955.

[22] J. Nash, "C^1 isometric imbeddings," *The Annals of Mathematics*, vol. 60, no. 3, pp. 383–396, 1954.

[23] J. Stoker, *Differential Geometry*. Pure and applied mathematics, Wiley, 1989.

[24] Y. Klein, S. Venkataramani, and E. Sharon, "Experimental study of shape transitions and energy scaling in thin non-Euclidean plates," *Physical Review Letters*, vol. 106, no. 11, p. 118303, 2011.

[25] T. Planchon, L. Gao, D. E. Milkie, M. W. Davidson, J. A. Galbraith, C. G. Galbraith, and E. Betzig, "Rapid three-dimensional isotropic imaging of living cells using Bessel beam plane illumination," *Nature Methods*, vol. 8, pp. 417–423, Jan. 2011.

[26] J. Arlt, V. Garcés-Chávez, W. Sibbett, and K. Dholakia, "Optical micromanipulation using a Bessel light beam," *Optics Communications*, vol. 197, no. 4-6, pp. 239–245, 2001.

[27] F. Courvoisier, J. Zhang, M. K. Bhuyan, M. Jacquot, and J. M. Dudley, "Applications of femtosecond Bessel beams to laser ablation," *Appl. Phys. A*, Sept. 2012.

[28] M. Mills, M. Kolesik, and D. Christodoulides, "Dressed optical filaments," *Optics letters*, vol. 38, no. 1, pp. 25–27, 2013.

[29] P. Polynkin, M. Kolesik, A. Roberts, D. Faccio, P. Di Trapani, and J. Moloney, "Generation of extended plasma channels in air using femtosecond Bessel beams," *Opt Express*, vol. 16, pp. 15733–15740, Sept. 2008.

[30] K. Stelmaszczyk, P. Rohwetter, G. Méjean, J. Yu, E. Salmon, J. Kasparian, R. Ackermann, J.-P. Wolf, and L. Woste, "Long-distance remote laser-induced breakdown spectroscopy using filamentation in air," *Applied Physics Letters*, vol. 85, no. 18, pp. 3977–3979, 2004.

[31] P. Rohwetter, K. Stelmaszczyk, L. Wöste, R. Ackermann, G. Méjean, E. Salmon, J. Kasparian, J. Yu, and J.-P. Wolf, "Filament-induced remote surface ablation for long range laser-induced breakdown spectroscopy operation," *Spectrochimica Acta Part B: Atomic Spectroscopy*, vol. 60, no. 7, pp. 1025–1033, 2005.

[32] L. Rayleigh, "Xxix. on images formed without reflection or refraction," *The London, Edinburgh, and Dublin Philosophical Magazine and Journal of Science*, vol. 11, no. 67, pp. 214–218, 1881.

[33] R. W. Gerchberg and W. O. Saxton, "Phase determination from image and diffraction plane pictures in the electron microscope," *Optik*, vol. 35, pp. 237–246, Jan. 1972.

[34] J. R. Fienup, "Phase retrieval algorithms: a comparison," *Applied Optics*, vol. 21, no. 15, pp. 2758–2769, 1982.

[35] D. Youla, "Mathematical theory of image restoration by the method of convex projections," *Image Recovery: Theory and Application*, pp. 29–77, 1987.

[36] H. H. Bauschke, P. L. Combettes, and D. R. Luke, "Phase retrieval, error reduction algorithm, and Fienup variants: a view from convex optimization," *JOSA A*, vol. 19, no. 7, pp. 1334–1345, 2002.

[37] J. Fienup and C. Wackerman, "Phase-retrieval stagnation problems and solutions," *JOSA A*, vol. 3, no. 11, pp. 1897–1907, 1986.

[38] C. Wackerman and A. Yagle, "Use of fourier domain real-plane zeros to overcome a phase retrieval stagnation," *JOSA A*, vol. 8, no. 12, pp. 1898–1904, 1991.

[39] M. Pasienski and B. Demarco, "A high-accuracy algorithm for designing arbitrary holographic atom traps," *Optics Express*, vol. 16, no. 3, pp. 2176–2190, 2008.

[40] D. E. Angelaki and B. J. Hess, "Self-motion-induced eye movements: effects on visual acuity and navigation," *Nature Reviews Neuroscience*, vol. 6, no. 12, pp. 966–976, 2005.

[41] D. E. Angelaki and K. E. Cullen, "Vestibular system: the many facets of a multimodal sense," *Annu. Rev. Neurosci.*, vol. 31, pp. 125–150, 2008.

[42] G. Yang and R. H. Masland, "Receptive fields and dendritic structure of directionally selective retinal ganglion cells," *Journal of Neuroscience*, vol. 14, no. 9, pp. 5267–5280, 1994.

[43] A. Cruz-Martín, R. N. El-Danaf, F. Osakada, B. Sriram, O. S. Dhande, P. L. Nguyen, E. M. Callaway, A. Ghosh, and A. D. Huberman, "A dedicated circuit links direction-selective retinal ganglion cells to the primary visual cortex," *Nature*, vol. 507, no. 7492, pp. 358–361, 2014.

[44] I. Eisenman and J. Wettlaufer, "Nonlinear threshold behavior during the loss of Arctic sea ice," *Proceedings of the National Academy of Sciences*, vol. 106, no. 1, pp. 28–32, 2009.

[45] I. Eisenman, "Factors controlling the bifurcation structure of sea ice retreat," *Journal of Geophysical Research: Atmospheres*, vol. 117, no. D1, 2012.

[46] L. Billings and E. Forgoston, "Seasonal forcing in stochastic epidemiology models," *Ricerche di Matematica*, vol. 67, no. 1, pp. 27–47, 2018.

[47] L. Gammaitoni, P. Hänggi, P. Jung, and F. Marchesoni, "Stochastic resonance," *Reviews of modern physics*, vol. 70, no. 1, p. 223, 1998.

[48] M. I. Freidlin, "Quasi-deterministic approximation, metastability and stochastic resonance," *Physica D: Nonlinear Phenomena*, vol. 137, no. 3-4, pp. 333–352, 2000.

[49] N. Berglund and B. Gentz, "Metastability in simple climate models: Pathwise analysis of slowly driven Langevin equations," *Stochastics and Dynamics*, vol. 2, no. 03, pp. 327–356, 2002.

[50] N. Berglund and B. Gentz, "A sample-paths approach to noise-induced synchronization: Stochastic resonance in a double-well potential," *The Annals of Applied Probability*, vol. 12, no. 4, pp. 1419–1470, 2002.

[51] S. Herrmann and P. Imkeller, "The exit problem for diffusions with time-periodic drift and stochastic resonance," *Annals of Applied Probability*, pp. 39–68, 2005.

[52] M. I. Freidlin, "The averaging principle and theorems on large deviations," *Russian mathematical surveys*, vol. 33, no. 5, p. 117, 1978.

[53] A. Y. Veretennikov, "On large deviations in the averaging principle for SDEs with a "full dependence"," *Annals of probability*, pp. 284–296, 1999.

[54] M. Dykman, H. Rabitz, V. Smelyanskiy, and B. Vugmeister, "Resonant directed diffusion in nonadiabatically driven systems," *Physical review letters*, vol. 79, no. 7, p. 1178, 1997.

[55] L. Onsager and S. Machlup, "Fluctuations and irreversible processes," *Physical Review*, vol. 91, no. 6, p. 1505, 1953.

[56] M. Chaichian and A. Demichev, *Path integrals in physics: Volume I stochastic processes and quantum mechanics*. CRC Press, 2018.

[57] M. I. Freidlin and A. D. Wentzell, *Random Perturbations of Dynamical Systems*, vol. 260. Springer Science & Business Media, 2012.

[58] D. Dürr and A. Bach, "The Onsager-Machlup function as Lagrangian for the most probable path of a diffusion process," *Communications in Mathematical Physics*, vol. 60, no. 2, pp. 153–170, 1978.

[59] T. Fujita and S.-i. Kotani, "The Onsager-Machlup function for diffusion processes," *Journal of mathematics of Kyoto University*, vol. 22, no. 1, pp. 115–130, 1982.

[60] H. W. Alt, L. A. Caffarelli, and A. Friedman, "Variational problems with two phases and their free boundaries," *Transactions of the American Mathematical Society*, vol. 282, no. 2, pp. 431–461, 1984.

[61] W. Moon and J. S. Wettlaufer, "A stochastic dynamical model of Arctic sea ice," *Journal of Climate*, vol. 30, no. 13, pp. 5119–5140, 2017.

[62] F. Yang, Y. Zheng, J. Duan, L. Fu, and S. Wiggins, "The tipping times in an Arctic sea ice system under influence of extreme events," *Chaos: An Interdisciplinary Journal of Nonlinear Science*, vol. 30, no. 6, p. 063125, 2020.

[63] K. S. Morupisi and C. Budd, "An analysis of the periodically forced pp04 climate model, using the theory of non-smooth dynamical systems," *IMA Journal of Applied Mathematics*, vol. 86, no. 1, pp. 76–120, 2021.

[64] M. di Bernardo, C. Budd, A. Champneys, and P. Kowalczyk, *Piecewise-smooth dynamical systems: theory and applications*, vol. 163 of *Applied Mathematical Sciences*. Springer Science & Business Media, 2008.

[65] M. di Bernardo, C. Budd, A. Champneys, P. Kowalczyk, A. Nordmark, G. Tost, and P. Piiroinen, "Bifurcations in nonsmooth dynamical systems," *SIAM Rev*, vol. 50, no. 4, pp. 629–701, 2008.

[66] A. Filippov, *Differential equations with discontinuous righthand sides*, vol. 18. Springer Science & Business Media, 2013.

[67] M. R. Jeffrey, "Hidden dynamics in models of discontinuity and switching," *Physica D: Nonlinear Phenomena*, vol. 273, pp. 34–45, 2014.

[68] D. D. Novaes and M. R. Jeffrey, "Regularization of hidden dynamics in piecewise smooth flows," *Journal of Differential Equations*, vol. 259, no. 9, pp. 4615–4633, 2015.

[69] M. R. Jeffrey, *Hidden Dynamics: The Mathematics of Switches, Decisions and Other Discontinuous Behaviour*. Springer, 2018.

[70] F. Pinski, A. Stuart, and F. Theil, "Gamma-limit for transition paths of maximal probability," *Journal of Statistical Physics*, vol. 146, no. 5, pp. 955–974, 2012.

[71] A. Braides, *Gamma-convergence for Beginners*, vol. 22. Clarendon Press, 2002.

[72] G. Dal Maso, *An introduction to Γ-convergence*, vol. 8. Springer Science & Business Media, 2012.

[73] E. Forgoston and R. Moore, "A primer on noise-induced transitions in applied dynamical systems," *SIAM Review*, vol. 60, no. 4, pp. 969–1009, 2018.

[74] C. K. Jones, "Geometric singular perturbation theory," in *Dynamical systems*, pp. 44–118, Springer, 1995.

[75] J. Harris and B. Ermentrout, "Bifurcations in the Wilson–Cowan equations with nonsmooth firing rate," *SIAM Journal on Applied Dynamical Systems*, vol. 14, no. 1, pp. 43–72, 2015.

[76] S. Wieczorek, P. Ashwin, C. Luke, and P. Cox, "Excitability in ramped systems: the compost-bomb instability," *Proceedings of the Royal Society A: Mathematical, Physical and Engineering Sciences*, vol. 467, no. 2129, pp. 1243–1269, 2010.

[77] P. Ashwin, S. Wieczorek, R. Vitolo, and P. Cox, "Tipping points in open systems: bifurcation, noise-induced and rate-dependent examples in the climate system," *Philosophical Transactions of the Royal Society A*, vol. 370, no. 1962, pp. 1166–1184, 2012.

[78] P. Ritchie and J. Sieber, "Early-warning indicators for rate-induced tipping," *Chaos: An Interdisciplinary Journal of Nonlinear Science*, vol. 26, no. 9, p. 093116, 2016.

[79] P. O'Keeffe and S. Wieczorek, "Tipping phenomena and points of no return in ecosystems: beyond classical bifurcations," *SIAM Journal on Applied Dynamical Systems*, vol. 19, no. 4, pp. 2371–2402, 2020.

[80] C. Kiers and C. K. Jones, "On conditions for rate-induced tipping in multi-dimensional dynamical systems," *Journal of Dynamics and Differential Equations*, vol. 32, no. 1, pp. 483–503, 2020.

[81] A. Hoyer-Leitzel and A. Nadeau, "Rethinking the definition of rate-induced tipping," *Chaos: An Interdisciplinary Journal of Nonlinear Science*, vol. 31, no. 5, p. 053133, 2021.

[82] N. Berglund and B. Gentz, "Beyond the Fokker-Planck equation: Pathwise control of noisy bistable systems," *Journal of Physics A*, vol. 35, no. 9, p. 2057, 2002.

[83] N. Berglund and B. Gentz, "Geometric singular perturbation theory for stochastic differential equations," *Journal of Differential Equations*, vol. 191, no. 1, pp. 1–54, 2003.

[84] N. Berglund and B. Gentz, *Noise-induced phenomena in slow-fast dynamical systems: a sample-paths approach*. Springer Science & Business Media, 2006.

[85] M. D. McDonnell, N. G. Stocks, C. E. M. Pearce, and D. Abbott, *Stochastic Resonance: From Suprathreshold Stochastic Resonance to Stochastic Signal Quantization*. Cambridge University Press, 2008.

[86] M. Dykman, P. McClintock, V. Smelyanski, N. Stein, and N. Stocks, "Optimal paths and the prehistory problem for large fluctuations in noise-driven systems," *Physical Review Letters*, vol. 68, no. 18, p. 2718, 1992.

[87] M. Dykman, E. Mori, J. Ross, and P. Hunt, "Large fluctuations and optimal paths in chemical kinetics," *The Journal of Chemical Physics*, vol. 100, no. 8, pp. 5735–5750, 1994.

[88] J. Lehmann, P. Reimann, and P. Hänggi, "Surmounting oscillating barriers," *Physical Review Letters*, vol. 84, no. 8, p. 1639, 2000.

[89] R. Maier and D. Stein, "Noise-activated escape from a sloshing potential well," *Physical Review Letters*, vol. 86, no. 18, p. 3942, 2001.

[90] M. Dykman, B. Golding, L. McCann, V. Smelyanskiy, D. Luchinsky, R. Mannella, and P. McClintock, "Activated escape of periodically driven systems," *Chaos: An Interdisciplinary Journal of Nonlinear Science*, vol. 11, no. 3, pp. 587–594, 2001.

[91] S. Wieczorek, C. Xie, and C. K. Jones, "Compactification for asymptotically autonomous dynamical systems: theory, applications and invariant manifolds," *Nonlinearity*, vol. 34, no. 5, p. 2970, 2021.

[92] K. Emanuel, "A fast intensity simulator for tropical cyclone risk analysis," *Natural hazards*, vol. 88, no. 2, pp. 779–796, 2017.

[93] A. Roberts, J. Guckenheimer, E. Widiasih, A. Timmermann, and C. K. Jones, "Mixed-mode oscillations of el nino–southern oscillation," *Journal of the Atmospheric Sciences*, vol. 73, no. 4, pp. 1755–1766, 2016.

[94] M. J. Keeling and P. Rohani, *Modeling infectious diseases in humans and animals*. Princeton University Press, 2011.

[95] T. Gross, C. D'Lima, J. Dommar, and B. Blasius, "Epidemic dynamics on an adaptive network," *Physical review letters*, vol. 96, no. 20, p. 208701, 2006.

[96] I. Z. Kiss, J. C. Miller, P. L. Simon, *et al.*, "Mathematics of epidemics on networks," *Cham: Springer*, vol. 598, 2017.

[97] H. W. Hethcote, "The mathematics of infectious diseases," *SIAM review*, vol. 42, no. 4, pp. 599–653, 2000.

[98] L. J. Allen, F. Brauer, P. Van den Driessche, and J. Wu, *Mathematical epidemiology*, vol. 1945. Springer, 2008.

[99] M. Martcheva, *An introduction to mathematical epidemiology*, vol. 61. Springer, 2015.

[100] F. Brauer, "Mathematical epidemiology: Past, present, and future," *Infectious Disease Modelling*, vol. 2, no. 2, pp. 113–127, 2017.

[101] F. Brauer, C. Castillo-Chavez, and Z. Feng, *Mathematical models in epidemiology*. Springer, 2019.

[102] W. O. Kermack and A. G. McKendrick, "A contribution to the mathematical theory of epidemics," *Proceedings of the royal society of london. Series A, Containing papers of a mathematical and physical character*, vol. 115, no. 772, pp. 700–721, 1927.

[103] T. Gross and H. Sayama, "Adaptive networks," in *Adaptive networks*, pp. 1–8, Springer, 2009.

[104] L. B. Shaw and I. B. Schwartz, "Fluctuating epidemics on adaptive networks," *Physical Review E*, vol. 77, no. 6, p. 066101, 2008.

[105] I. B. Schwartz and L. B. Shaw, "Rewiring for adaptation," *Physics*, vol. 3, no. 17, 2010.

[106] V. Marceau, P.-A. Noël, L. Hébert-Dufresne, A. Allard, and L. J. Dubé, "Adaptive networks: Coevolution of disease and topology," *Physical Review E*, vol. 82, no. 3, p. 036116, 2010.

[107] S. L. Feld, "Why your friends have more friends than you do," *American journal of sociology*, vol. 96, no. 6, pp. 1464–1477, 1991.

[108] T. House, G. Davies, L. Danon, and M. J. Keeling, "A motif-based approach to network epidemics," *Bulletin of Mathematical Biology*, vol. 71, no. 7, pp. 1693–1706, 2009.

[109] C. Nowzari, V. M. Preciado, and G. J. Pappas, "Analysis and control of epidemics: A survey of spreading processes on complex networks," *IEEE Control Systems Magazine*, vol. 36, no. 1, pp. 26–46, 2016.

[110] P. Van Mieghem and R. van de Bovenkamp, "Accuracy criterion for the mean-field approximation in susceptible-infected-susceptible epidemics on networks," *Physical Review E*, vol. 91, no. 3, p. 032812, 2015.

[111] M. J. Keeling, "The effects of local spatial structure on epidemiological invasions," *Proceedings of the Royal Society of London. Series B: Biological Sciences*, vol. 266, no. 1421, pp. 859–867, 1999.